Department of Mechanical Engineering
Penn State University
University Park, PA 16802

Report PSGDL-R-92/93-0002

An Experimental Study of the Sources of Fluctuating Pressure Loads Beneath Swept Shock/Boundary-Layer Interactions

by

G. S. Settles and S. Garg

Final Technical Report on NASA Grant NAG-1-1070
for the Period January 1, 1990 - December 31, 1992

Submitted to:

Dr. William Zorumski, Grant Monitor
NASA-Langley Research Center, MS-462
Hampton, VA 23665-5225

April, 1993

Penn State Gas Dynamics Laboratory
303 Mechanical Engineering
University Park, PA 16802

Wall Pressure Fluctuations Beneath Swept Shock Wave/Boundary Layer Interactions

S. Garg and G. S. Settles
Penn State University, University Park, PA 16802

ABSTRACT

An experimental research program providing basic knowledge and establishing a database on the fluctuating pressure loads produced on aerodynamic surfaces beneath three-dimensional shock wave/boundary layer interactions is described. Such loads constitute a fundamental problem of critical concern to future supersonic and hypersonic flight vehicles. A turbulent boundary layer on a flat plate is subjected to interactions with swept planar shock waves generated by sharp fins at angle of attack. Fin angles from 10° to 20° at freestream Mach numbers of 3 and 4 produce a variety of interaction strengths from weak to very strong.

Miniature Kulite pressure transducers flush-mounted in the flat plate are used to measure interaction-induced wall pressure fluctuations. The distributions of properties of the pressure fluctuations, such as their rms levels, amplitude distributions and power spectra, are also determined. Measurements have been made for the first time in the aft regions of these interactions, revealing fluctuating pressure levels as high as 160 dB. These fluctuations are dominated by low frequency (0-5 kHz) signals. The maximum rms levels in the interactions show an increasing trend with increasing interaction strength. On the other hand, the maximum rms levels in the forward portion of the interactions decrease linearly with increasing interaction sweepback. These rms pressure distributions and spectra are correlated with the features of the interaction flowfield.

The unsteadiness of the off-surface flowfield is studied using a new, non-intrusive technique based on the shadowgraph method. The results indicate that the entire lambda-shock structure generated by the interaction undergoes relatively low-frequency oscillations. Some regions where particularly strong fluctuations are generated have been identified.

Fluctuating pressure measurements are also made along the line of symmetry of an axisymmetric jet impinging upon a flat plate at an angle. This flow was chosen as a simple analog to the impinging jet region found in the rear portion of the shock wave/boundary layer interactions under study. It is found that a sharp peak in rms pressure level exists at or near the mean stagnation point. It is suggested that the phenomena responsible for this peak may be active in the swept interactions as well, and may cause the extremely high fluctuating pressures observed in the impinging jet region in the present experimental program.

INTRODUCTION

Much effort has gone into the study of shock wave/boundary layer interactions (SWBLIs) over the past few decades. This class of flows, besides representing a fundamental fluid dynamics problem, is also of significant practical importance since SWBLIs are ubiquitous on the aerodynamic control surfaces and in the propulsion systems of high speed flight vehicles. One of the most commonly studied SWBLIs is that generated by a sharp fin at angle of attack, α, mounted perpendicular to a flat test surface. The fin generates a swept, planar shock wave which interacts with the zero-pressure-gradient boundary layer on the test surface. Recent studies have provided extensive knowledge about the mean surface properties[1-3] and the flowfield[4] of this sharp-fin interaction. Much of this information is summarized in the reviews by Settles and Dolling.[5,6]

The most salient feature of this interaction is its *quasiconical* nature. This has been observed by many investigators and recently confirmed by parametric studies.[1,4,7] The interaction growth is found to be essentially conical except for an initial region in the immediate vicinity of the juncture of the fin leading-edge and the flat plate. The topological features of the outboard flow thus appear to emanate from a single point, which has been termed the "Virtual Conical Origin" (VCO). Due to the quasiconical nature of the interaction, the most appropriate coordinate system for its study is a spherical polar system with its origin located at the VCO. Such a coordinate frame is shown in Fig. 1.

Figure 2 shows a sketch of the limiting streamlines (*i.e.* the surface flow pattern) beneath the interaction. The initial non-conical region is characterized by the *inception length* (L_i). Other features are indicated in the figure by their angular location (angular measure being the only meaningful descriptor of a conical flow). These are: upstream influence (U), primary separation (S_1), secondary separation (S_2) and primary attachment (A_1). The undisturbed "inviscid" shock angle is labeled β_0, and the angle of attack of the fin is α.

Due to the quasiconical nature of this flowfield, a simplification widely used is to project it onto a unit sphere centered at the VCO. This allows the flow to be viewed in two dimensions and greatly simplifies its analysis. Figure 3 shows such a projection. The off-surface features of the flowfield are sketched, including the inviscid shock wave, the separation shock, the incoming boundary layer and separated free shear layer, the separation bubble, the rear shock (which turns the separated shear layer back toward the flat plate), the attachment of the boundary layer and the "slip line" emanating from the triple-point intersection of the three shock waves.

There exists a body of evidence indicating that such SWBLIs are unsteady when the incoming boundary layer is turbulent, but relatively little is known about the nature and causes of this unsteadiness. Due to this inherent unsteadiness, SWBLIs can generate significant surface pressure fluctuations. These fluctuating pressure loads are especially significant in that they can occur in conjunction with high aerothermal loads, and can pose a threat to the structural integrity of flight vehicles.

Much of the evidence about the unsteady behavior of SWBLIs is from optical results, *eg.* high-speed cinema records, and is mostly qualitative. The available quantitative measurements come from flush-mounted wall pressure transducers which do not disturb the flowfield. To date, nearly all of such work has involved 2-D interactions. These include

unswept compression ramps,[8,9] the symmetry planes of unswept blunt fins,[10] forward-facing steps,[11] etc. Only recently have measurements been made in swept shock/boundary layer interactions.[12-14] However, there are indications that many of the basic phenomenological features here are similar to those of 2-D interactions.

A characteristic feature observed in the 2-D interactions is the intermittent back-and-forth motion of the separation shock.[8] This gives rise to a bi-modal wall pressure signal near separation. These two states correspond to the undisturbed boundary layer signature (when the shock is downstream of the transducer) and the higher pressure behind the shock (when it is upstream of the transducer). This causes a sharp rise in fluctuation intensity at separation, represented, for example, by the rms of the instantaneous wall pressure. Tran[12] measured wall pressure fluctuations in a Mach 3 interaction generated by a sharp fin at several angles of attack. He reported that, for his two strongest interactions, the wall pressure signal near separation exhibited large-amplitude intermittent fluctuations indicating a translating separation shock wave.

Two more-recent experiments measured wall pressure fluctuations in a Mach 5 sharp fin interaction: Gibson's[13] measurements indicated only the presence of a quasi-steady "shuddering" compression system rather than a translating separation shock wave. However, further experiments by Schmisseur and Dolling,[14] which were carried out in the same facility at the same Mach number and fin angles as Ref. 13, indicated that a translating separation shock was indeed present. The only difference between these two experiments is that the latter involved an incoming boundary layer more than twice as thick as that of the former. The larger transducer diameter relative to the boundary layer thickness in Gibson's experiments is believed to be the cause of this difference. More will be said about this issue in the discussion of the present results.

The goal of the current study is to assess the acoustic loads generated by a sharp-fin-generated swept SWBLI and to gain a better understanding of the mechanisms involved in their generation. Also, earlier studies of this interaction have concentrated on the forward portion of the interaction (near separation) while neglecting aft locations close to the fin/plate junction. In the present experiments, measurements of surface pressure fluctuations are made from front to back of the interaction, taking advantage of its quasiconical symmetry. Finally, the present study bridges the Mach number gap between the previous measurements, since it is conducted at Mach 3 and 4 for a range of interaction strengths.

EXPERIMENTAL METHODS

Facilities

The experiments were performed in both the supersonic wind tunnel facility and the freejet facility of the Penn State University Gas Dynamics Laboratory. The wind tunnel is an intermittent blowdown type with a test section size of 150 × 170 × 600 mm and a variable Mach number capability over the range of Mach 1.5-4.0. A 57 m^3, 2000 kPa pressure reservoir provides testing times up to 2 min. at stagnation pressures up to 1500 kPa.

The freejet facility can eject subsonic or supersonic flows into the atmosphere using various axisymmetric, method-of-characteristics nozzles. This facility provides essentially-

continuous testing times and unlimited optical access. The freejet facility can use as its gas supply either bottled gas or the same reservoir as the supersonic wind tunnel facility. A non-venting regulator maintains nearly-constant total pressure conditions in the 50.8 mm diameter stilling chamber. The stilling chamber contains a baffle plate to spread the flow entering from the 19.05 mm inlet pipe, a set of screens for flow conditioning, and a port for measuring the total temperature and total pressure.

Experimental Setup

Fin-Generated Interactions

For the present tests, a flat plate 508 mm long, spanning the tunnel, was mounted in the test section to provide the interaction test surface. A 2-D, equilibrium, nearly adiabatic, zero-pressure-gradient boundary layer forms on this plate[1] with natural transition typically occurring within 10 mm of the leading edge. A fin model with a 10 deg. sharp leading edge was placed with its tip 216 mm from the plate leading edge and 26.2 mm from the tunnel sidewall. The fin was 120 mm long and 73 mm high. The height of the fin was sufficient to ensure that the interaction was semi-infinite (*i.e.* independent of fin height). A pneumatic fin-injection mechanism was employed to hold the fin tightly onto the flat plate and to position the fin to the desired angle of attack. Teflon tape attached to the bottom of the fin prevented leakage underneath it during the tests, and also avoided metal-to-metal contact during fin motion.

A simplification afforded by the quasiconical nature of the interactions under study is that their surface properties outside the inception zone can be completely characterized by making measurements along an arc centered at the VCO (such as that formed by the intersection of the unit sphere with the test surface in Fig. 3). However, since the location of the VCO lies in the vicinity of the fin leading edge but varies with interaction strength, in the present experiments the measurement locations are simply arrayed along an arc centered at the fin leading edge as a first approximation. Transducer ports are provided in the flat plate at 2 deg. angular separation from 8 deg. to 70 deg. with respect to the freestream direction. Figure 4 shows a schematic of the arrangement. No attempt was made to optimize transducer placement for any particular interaction. The locations of the VCO being known from previous studies,[1,4] the angular positions of the transducers were later corrected from fin leading edge to VCO. In the remainder of this article, wherever angular distributions of measured quantities are presented, this corrected (VCO-based) angle is used.

In order to correlate the measured wall pressure fluctuations with knowledge of the structural unsteadiness of the flowfield, the interaction was also studied using a non-intrusive optical method. By optically sensing the motion of flowfield features, we expect to gain insight into the overall unsteadiness of the flowfield. The experimental technique, called "optical deflectometry," was developed in-house[15] and has been used previously to investigate the structure of turbulence in a compressible mixing layer.[16]

The optical arrangement for the measurements is shown in Figure 5. A conical beam of continuous white light is focused at the VCO of the swept interaction and directed along the interaction sweep line. This beam exits the wind tunnel test section through a full-coverage acrylic window, whereupon it strikes a ground-glass screen. With proper beam

alignment, a real-time shadowgram image is cast on the ground-glass. Alternatively, the image can be recorded on film by using a camera in place of the ground-glass.

Alvi and Settles[17] used this technique to provide detailed flowfield information about swept interaction flowfields. Figure 6 shows a still image from Ref. 17 as an illustration of the level of detail that can be visualized. The image shown was obtained by using a strobed light source with a pulse duration of the order of 10-15 microseconds. This essentially "freezes" the flow and the unsteadiness is apparent from an examination of a series of successive frames. However, due to the limitations of the standard video format used for recording, successive frames are spaced 1/30th of a second apart. Therefore, a series of frames is a discretely-sampled representation of the randomly fluctuating flowfield, rather than a continuous one. In our case, a continuous-light source was used and a fiber-optic pickup/cable was employed to sense fluctuations of light intensity on the ground-glass and convey them to a rapid-response photomultiplier tube (PMT). The output of the PMT was sampled and stored by a high-speed data acquisition system. The signal thus obtained was a time-trace of the light intensity at the position of the fiber-optic pickup. The ground-glass screen was mounted on a traversing mechanism, which allowed the fiber-optic pickup to be positioned at any desired point in the field of view. Figure 7 shows an image of the interaction as cast on the ground-glass screen. Also seen in the figure are a grid superimposed upon the image for accurate positioning of the fiber-optic pickup, the fiber-optic pickup/cable, and the measurement locations. The grid lines seen in Figure 7 are spaced 5 mm apart.

Impinging Jet Measurements

Previous studies[1-3] of fin-generated interactions have observed peaks in the distributions of surface pressure, heat transfer, and skin friction in the region near the fin-plate junction. In the present study, similar peaks in the distribution of rms pressure fluctuations were observed in this region. The flowfield model of Alvi and Settles[4] denotes this as the "impinging-jet" region. Briefly, they found that the streamtube processed by the separation and rear shocks below the triple point turns toward, and attaches to, the flat-plate surface near the foot of the fin. Aft of the inviscid shock, this streamtube is bounded by the slip-line and the separation bubble, and resembles a jet impinging upon the plate surface. Alvi and Settles[4] have further suggested that the stagnation of this jet on the flat plate is responsible for the observed peaks in surface properties.

Measurements of fluctuating pressures were made along the line of symmetry of an axisymmetric jet impinging upon a flat plate at an angle. This flow was chosen as a simple analog to the impinging-jet region found in the rear portion of the shock wave/boundary layer interactions under study. By studying this simplified flowfield, we hoped to gain a better understanding of the physics involved in the generation of high levels of pressure fluctuations in the rear portion of the SWBLIs under study.

The freejet facility described above was used for these tests. The flat-plate used for the wind-tunnel tests was also used here as the impingement surface. A single pressure transducer was mounted in one of the available ports and the plate was positioned 4 jet diameters downstream of the nozzle exit. Figure 8 shows a schematic of the arrangement used. It shows a cross-sectional view through the center of the nozzle. The plate was mounted on a bench which could be traversed in both the x and y-directions. The single

pressure transducer was positioned at a desired point along the line of symmetry by traversing the plate and bench rather than by moving the transducer to a different port in the flat-plate. Surveys were therefore completed in multiple runs, during which the flow conditions were kept constant.

Test Conditions

The nominal Mach numbers of the present wind-tunnel experiments were 3 and 4. The approximate stagnation chamber pressure and temperature were 965 kPa and 300 K for Mach 3, and 1655 kPa and 300 K for Mach 4. The freestream Reynolds number was 67 × 10^6 m^{-1} and 75 × 10^6 m^{-1} for Mach 3 and 4, respectively.

Detailed pitot pressure surveys of the boundary layer have shown that it is two-dimensional and that its mean velocity profile closely matches the compressible law of the wall/law of the wake.[1] At the location of the fin leading edge, $\delta \approx 3.5$ mm, $\delta^* \approx 1.12$ mm, and $\theta \approx 0.13$ mm. The flat plate has a negligible pressure gradient along its length and is in a near-adiabatic condition during the experiments.

The test cases were chosen to span a wide range of interaction strengths. Previous investigators have found that important features of swept SWBLIs scale with the strength of the inviscid shock wave, which can be represented either by the Mach number normal to the shock (M_n), or by the pressure rise across it (p_2/p_1). The values of these parameters for the present cases are tabulated below.

M_∞	α	M_n	p_2/p_1
3.0	10°	1.40	2.120
	16°	1.64	2.971
	20°	1.85	3.826
4.0	16°	1.89	4.001
	20°	2.16	5.227

Of these cases, only the $M_\infty = 4$, $\alpha = 20^\circ$ interaction was investigated using the optical deflectometry technique described above.

For the impinging jet measurements, the freejet facility was used with a Mach 1.65 method-of-characteristics nozzle. This Mach number was chosen because it was close to the estimated Mach number of the impinging jet in the $M_\infty = 4$, $\alpha = 20^\circ$ interaction. The stagnation pressure was about 440 kPa (64 psi) such that the jet, which exited into ambient air, was approximately perfectly expanded. The stagnation temperature for the experiments was about 300 K. The values of the angle of impingement of the jet, α, were 30°, 40°, 50° and 60°. These values were chosen to encompass the jet-impingement angles in the swept SWBLI cases listed in the table above, which were estimated from the flowfield maps of Alvi and Settles.[4]

Instrumentation, Signal Conditioning and Data Acquisition

Fluctuating-Pressure Measurements

The pressure transducers used in the experiments are commercially-available miniature devices manufactured by Kulite Semiconductor Products, Inc. (model XCQ-062-50A). They have a pressure-sensitive area 0.71 mm in diameter and an outer case diameter of 1.63 mm. According to the manufacturer's specifications, these transducers have a natural frequency of approximately 500 kHz, but due to the presence of perforated screens above the diaphragm which protect it from damage due to dust particles in the flow, the frequency response is limited to about 50 kHz. The sensitivity of the transducers is typically 0.4-0.6 mV/kPa (3-4 mV/psi). The transducers were calibrated statically using a Wallace & Tiernan model 61A-1A-0100 pressure gauge.

The pressure transducer output was amplified and low-pass filtered using Precision Filters model 6602B-I-LP1 filters prior to digitization. LeCroy model 6810 Waveform Recorders with 12-bit resolution were then used to digitize and record the signals. The sampling frequency was 100 kHz and the low-pass filter cutoff frequency was 45 kHz. Six transducers were used in each test, and the signals from them were simultaneously sampled and recorded. For each channel, 128 records of 1024 points were acquired, yielding a total of 131,072 data points per channel per tunnel run. This sample size was large enough to ensure convergence of its statistics.

A simple test was devised to assess the magnitude of electronic noise present in these signals. Data were acquired with the transducers exposed to a constant pressure (so that, ideally, no fluctuations should be recorded), keeping the instrumentation settings the same as for the actual tests. These data were then processed in the same fashion as actual fluctuating pressure data. The rms "noise-pressure" level was then compared to the rms level measured beneath the undisturbed boundary layer. The noise rms was found to be approximately one-fifth of the rms level underneath the Mach 4 boundary layer. This represents a worst case scenario; the rms pressure beneath the Mach 3 boundary layer was twice as high as the Mach 4 case (due to the higher static pressure for Mach 3), and the rms levels beneath the corresponding interactions were higher still. Therefore, the signal-to-noise ratio (SNR) was greater than five in all cases.

Optical Deflectometry Measurements

As shown in Figure 5, a fiberoptic pickup/cable was used to sense the illumination at a given point in the conical shadowgram and to convey it to a photomultiplier tube (PMT). The PMT (Hammamatsu R928), converted these illumination levels to analog signals which were digitized and recorded by the data acquisition system described above. The number of samples recorded was the same as for the pressure measurements.

The PMT was operated in a range in which its voltage output varies linearly with the intensity of incident light. The frequency response of the PMT is essentially unlimited and flat well into the MHz range of frequencies. However, due to the presence of unexplained sources of noise in the 70-80 kHz range, it was necessary to low-pass filter the PMT output above 65 kHz, and the signal was then sampled at 200 kHz. In order to avoid fluctuations in light intensity at line frequency, a halogen bulb powered by a DC supply was used as the light source.

The output of the PMT in the present experiments is proportional to the light intensity at the location of the fiberoptic pickup in the shadowgram, which in turn is proportional to the second spatial derivative of density at that point. The purpose of these experiments was not to measure any conventional physical flowfield variable. Rather, they were primarily intended to optically detect the motion of flowfield structures and disturbances in the interaction. This is made possible by the fact that such flow features and acoustic disturbances are rendered visible in a shadowgram due to the density gradients associated with them. The magnitude of fluctuations of the PMT signal, as represented by its rms value for example, is a measure of the fluctuating energy of these disturbances.

The noise inherent in the PMT is broadband and increases in proportion to the incident light intensity. It was found during the course of the experiments that the rms level of fluctuations recorded at any given point also increased approximately linearly with the mean light intensity at that point. Since the illumination level was not uniform over the whole shadowgram (as can be seen in Fig. 7), the measured rms level was normalized by the mean value in order to remove this inherent bias. No attempt was made to calibrate and convert the voltages recorded to units of light intensity since it is the temporal behavior of the light fluctuations that is of interest, not the optical intensity itself.

RESULTS & DISCUSSION

Incoming Boundary Layer Measurements

The probability density distributions of the incoming boundary layer pressure fluctuations were essentially Gaussian. The present power spectra agreed qualitatively with previously published results.[12-14] The rms of the wall pressure fluctuations normalized by the freestream static pressure, σ_p/P_∞ was determined to be 0.013 ± 0.001 for Mach 3, and 0.0115 ± 0.001 for Mach 4. These values are somewhat low compared with the semi-empirical prediction of Laganelli *et al*[18] (σ_p/P_∞ = 0.023 and 0.03 for Mach 3 and 4 respectively), but agree well with the Mach 3 measurements of Tan *et al*[19] (σ_p/P_∞ = 0.013 ± 0.0005) and those of Dolling and Or[9] (σ_p/P_∞ = 0.016 ± 4%). Experimental data generally tend to fall below the predicted values. This is due to the finite size of the transducers used, which are "large" compared to the length scales of the fine-scale turbulent structures in the boundary layer, thus tending to eliminate the contributions of high frequency fluctuations. Moreover, the incoming boundary layer has significant energy above the filter cutoff frequency (about 45 kHz) since a typical large eddy frequency in the present experiments is 200 kHz (U_e/δ). However, since the pressure fluctuations inside the interactions themselves are dominated by relatively low frequencies, this is not considered to be a serious limitation of the present experimental program. In other words, our emphasis is not on the incoming boundary layer or the separation location at the beginning of the interaction.

Interaction Measurements

RMS Distributions

Distributions of the rms pressure fluctuation level, σ_p, along with the corresponding mean

pressure distributions are presented in Figure 9 for M=3 and 4, $\alpha = 16$ and 20 deg. These rms values are shown twice, being normalized by both the freestream pressure (P_∞) and the local mean pressure (P_w). The flowfield maps constructed by Alvi and Settles[4] for these cases are also shown. Note that the flowfield maps are drawn on the same scale as the rms and mean pressure distributions, facilitating visual comparison of the three. Some features of these distributions are described below.

When normalized by the local mean pressure, the rms distributions display features that are apparently universal in SWBLIs - both 2-D and 3-D. One of these is the peak observed at separation. However, in 2-D interactions, the magnitude of this peak is much larger (as much as 25% of the local mean pressure) than in swept interactions. This peak is widely believed to be caused by the intermittent motion of the separation shock. Its low present value (0.039 max.) suggests that intermittency may be less pronounced in swept interactions. However, the values measured by Tran[12] in swept interactions with the same Mach number and fin angle were almost twice as high. The comparatively-low values measured in this study are probably due to a spatial resolution problem suffered by the present measurements, as will be explained in the next section.

Aft of the separation peak, the rms level is observed to drop and remain relatively constant for some angular distance. This region approximately corresponds to the so-called "plateau region" in the mean pressure distributions. Examination of the flowfield maps reveals that there are no significant changes in the flowfield (both on and off the surface) over much of this region.

The next feature in the rms distributions of Fig. 9 is the appearance of a second peak downstream of the first. This occurs in the vicinity of the "dip" in the mean pressure distribution. The magnitude of this peak is approximately the same as that of the peak associated with separation. It can be seen that this downstream fluctuating pressure peak lies directly beneath the core of the separation vortex. This is observed in all the present test cases and is believed to be the cause of the peak in the rms level.

The data presented in Ref. 14 also exhibit this peak, although in their case it is located *upstream* of the inviscid shock wave, which is more highly swept due to their larger Mach number. In the absence of flowfield visualization of the Mach 5 interactions, definite conclusions cannot be drawn from this observation. However, it does offer a clue as to the possible development of the off-surface flowfield structure as Mach number is increased. From the flowfield maps shown in Fig. 9, it can be seen that the inviscid shock position and the vortex core grow closer together as the interaction strength is increased. It is believed to be possible that this trend continues such that, for very strong interactions, the separated vortex core actually lies upstream of the inviscid shock position.

The highest raw pressure fluctuation levels are observed at locations close to the fin (this region had been neglected in earlier studies) in the impinging-jet region. A peak in rms level is observed slightly upstream of the location of primary attachment in all cases except the Mach 4, $\alpha = 20^\circ$ case. We believe this is caused by a random motion of the attachment line. This phenomenon will be discussed along with the presentation of the results of the impinging jet experiments. Aft of this peak, the rms level decreases, and is seen to rise again at locations closest to the foot of the fin. This rise in fluctuation intensity is believed to be due to the "flapping" motion of the slip line, which was observed by Alvi and Settles.[4] The highest rms level recorded in these experiments is 0.32 psi in the Mach 3, $\alpha = 20^\circ$ case,

which corresponds to a sound pressure level of 160 dB (referenced to 20 μPa absolute). This fluctuating pressure level is approximately 10% of the freestream static pressure (3.2 psia at Mach 3). This places such interactions in the category of significant acoustic-load generators.

The maximum value of σ_p/P_∞ is plotted versus the Mach number normal to the inviscid shock (M_n) in Figure 10. Previous investigators[4] have found M_n to be the best overall parameter to describe the interaction strength. Here one observes the general trend that a rise in fluctuation intensity occurs with rising interaction strength as denoted by M_n.

Figure 11a shows a plot of the magnitude of the fluctuating pressure peak near primary separation versus the angle of the primary separation line (β_{s1}). There appears to be a roughly-linear correlation between these two quantities. The greater the separation-line angle (*i.e.* the less swept-back the interaction), the higher the fluctuation intensity. Schmisseur and Dolling's[14] compilation of data from their own sharp fin experiments, Tran's[12] sharp fin experiments at Mach 3, and the swept compression ramp data of Erengil and Dolling[20] all showed a similar quasi-linear correlation between the maximum rms pressure level in the intermittent region and the separation line sweepback angle.

In Fig. 11b, the peak fluctuation value near S_1 is next plotted versus (β_0-μ_∞), which is a "reduced" shock strength parameter that takes into account the effect of freestream Mach number on shock strength (here, μ_∞ is the Mach angle of the freestream). The collapse of the data onto a single line is somewhat better in Fig. 11b than in Fig. 11a. The identification of the parameters that control the magnitude of pressure loads in these interactions is not considered to be completed by Figs. 11, but it is a beginning.

Probability Density Distributions

The probability density functions (pdf's) of the pressure fluctuations are expected to be of interest mainly in the forward portion of the interaction, near separation. This is because an intermittent signal, such as may be caused by a translating separation shock, has a distinctly non-Gaussian pdf[8,12,14] which may be highly skewed or bi-modal. In the present study - for all the cases tested - the pdfs were found to be essentially Gaussian *throughout* the interaction. Even close visual inspection of raw pressure-time histories does not reveal any evidence of intermittency in the present data. Of the three other existing studies of pressure fluctuations in sharp fin interactions, two (Refs. 12 and 14) found evidence of intermittent separation. The other experiments (Ref. 13) found no such evidence.

We believe we have identified the reason for this discrepancy. The experiments which do not exhibit intermittent separation were conducted beneath a relatively-thin flat-plate boundary layer, whereas the other two experiments used a tunnel-floor boundary layer which is an order of magnitude thicker. In the present study, the flat-plate boundary layer thickness is less than twice the transducer diameter. Now, if the typical length scale of the region within which the separation shock oscillates (called L_{shock} by some investigators) is of the same order of magnitude as the boundary layer thickness, it might very well happen that this region either falls between two adjacent transducers or else completely on the face of one transducer in the "thin" boundary layer cases. In either case the pressure signal thus recorded will not show intermittency, even if it is actually present in the flow. (It should be noted that a direct scaling relationship between L_{shock} and the boundary layer thickness has not been demonstrated,[9] though it is known that these two length scales are always at least

of the same order of magnitude).

Thus, the explanation of the discrepancy in pressure-fluctuation intermittency found in Refs. 12-14 and the present work is that it is essentially a resolution problem with the thin-boundary-layer experiments. This also explains the lower rms levels recorded near separation in the current study, compared to those of previous experiments using thicker boundary layers.

Power Spectra

Figure 12 presents the power spectra from the present Mach 4, $\alpha = 20^{\circ}$ interaction at locations ranging from the undisturbed boundary layer to the fin/plate junction. These spectra are representative of the trends observed in all the other interaction cases studied. The corresponding flowfield map can be seen in Fig. 9. The abscissa of Fig. 12 is the "raw" power spectral density (PSD) plotted on a logarithmic scale. (The conventional practice of normalizing the PSD by the rms level has deliberately not been followed here in order to show more clearly the evolution of the energy content of different frequency ranges through the interaction).

As expected, the incoming boundary layer spectrum in Fig. 12 is broadband and approximately flat up to the filter cutoff frequency of about 45 kHz. Note that there is significant energy above the cutoff, as mentioned earlier. However, since the present focus of interest is on the higher-amplitude, lower-frequency fluctuations in the interaction, this is not a serious limitation.

Near primary separation (Fig. 12b), a dramatic increase in energy up to about 30 KHz is observed. This is thought to be due to the motion of the separation shock. Further downstream, under the separation bubble, the spectrum "relaxes" back to its original shape, but with increased energy content over the entire range of frequencies measured (Figs. 12c-f). This is reflected in the elevated rms levels also seen at these locations (see Fig. 9). Referring to the flowfield map in Fig. 9, one sees no new flow features for some angular distance downstream of primary separation, and the spectrum shape remains approximately the same in this region.

Then, as the location of "secondary separation" is approached ($\beta = 37$ deg., Fig 12h), an increase in energy is observed in the frequency range 0-15 KHz. In their conical shadowgraphy experiments, Alvi and Settles[4] observed significant optical disturbances in the flowfield near secondary separation, but its exact nature was not clear. They also concluded that only *incipient* secondary separation occurred under present conditions.

At locations still further aft, in the "impinging jet" region (Figs. 12l-n), there is a shift in spectral energy from high- to low-frequency fluctuations. It is suggested that this is due to the fact that these locations are relatively isolated from the influence of the turbulent separated shear layer, which wraps around the vortex core and becomes a part of the reverse flow upstream of these locations (see flowfield map in Fig. 9). Visually, the small-scale turbulence of the free shear layer never extends aft of about $\beta = 28^{\circ}$ in the Mach 4, $\alpha = 20^{\circ}$ interaction.

The spectra closest to the fin/plate junction, where the highest rms levels were measured, are dominated by very low frequencies in the range 0-5 kHz (Figs. 12o,p). As mentioned above, it is possible that this is due to the "flapping" motion of the slip line, which was observed by Alvi and Settles.[4]

Coordinate Frame of Fluctuation Spectra

The axes used to plot the power spectra presented above are different from those conventionally used by previous authors.[12-14] In these previous studies, the quantity $fG(f)/\sigma_p^2$ is plotted vs. f on a linear-log scale, where f is the frequency, $G(f)$ the power spectral density at frequency f, and σ_p^2 is the variance of the fluctuations. When plotted on these axes, a power spectrum has an area under it equal to unity. Also, the area under a given curve segment is linearly proportional to the contribution of that frequency range to σ_p^2. However, Dolling and Dussauge[21] have pointed out the drawbacks of this approach and have suggested that care must be taken in the interpretation of such spectra. Due to the logarithmic abscissa, the magnitude of the frequency range spanned by two curve segments of equal width but located at different center frequencies is different. The curve segment at the higher center frequency spans a much larger range of frequencies than does the one at the lower center frequency. This is illustrated in Figure 13a. In Figure 13b, the same spectrum shown in Fig. 13a is plotted as $G(f)$ vs. f on log-linear axes. The spectrum shown in these Figs. is the same as Fig. 12b (*i.e.* near primary separation in the Mach 4, $\alpha = 20^\circ$ interaction). It can be seen that what appears to be a dominant peak around 7 kHz in Fig. 13a is barely noticeable in Fig 13b. Thus, we believe that plotting $fG(f)/\sigma_p^2$ vs. f can be misleading, and have thus chosen to show the present power spectra in the $G(f)$ vs. f log-linear coordinate frame.

Supplementary Experiments

The optical deflectometry and impinging jet experiments were carried out to supplement the results of the unsteady pressure measurements described above. The results of these two experiments will be described briefly here; they will be dealt with in greater detail in the first author's doctoral dissertation, which should be available in a few months' time.

Optical Deflectometry

RMS Distributions

Figure 14 shows the distribution of rms light-intensity (normalized by the mean level) along rows A, B, D and E (refer to Fig. 7 for row locations). The abscissa is the horizontal distance, in centimeters, along the row from the leftmost measurement location. Thus, distances are measured from location A1 in Fig. 14a, and from location D1 in Fig. 14c, for example. Selected measurement location numbers are also shown in Fig. 14 for reference.

Row A is located above the triple-point and cuts across the "main" shock wave. It can be seen that the fluctuation level is relatively constant in the freestream flow upstream of the shock, and reaches approximately the same level far downstream of it. The rms level increases in the vicinity of the shock wave. This is an indication of shock oscillation since motion of the (dark) shock across the measurement location causes larger variations in light intensity than do turbulent fluctuations in the freestream, for example. It should be noted here that what appears to be a "twin peak" distribution with peaks immediately upstream and downstream of the shock is actually a single peak. The locations embedded in the shadow of the shock wave (locations 7 and 8 in Fig. 14a) record lower rms levels because the shock wave never completely moves across them. This is due to the finite thickness of

the shock wave in the shadowgram - a limitation of any practical shadowgraphy arrangement. A dashed line in Fig. 14 shows the expected behavior of the true rms distribution.

The rms distribution along row B is very similar to that along row A. The rms levels at both extremes of the row are approximately the same as for corresponding locations in row A. There is again a rise in fluctuation intensity in the vicinity of, and across the triple-point of the λ-shock structure. However, the peak is larger in magnitude, indicating the presence of stronger fluctuations.

Row D passes through the separation and rear shock waves, and its downstream end is just aft of the slip-line. The rms distribution for this row is shown in Fig. 14c. Proceeding along row D from right-to-left (in the direction of the flow), a sharp peak is observed immediately downstream of the separation shock (location 25). In the region between the separation and rear shocks, the rms level is approximately constant but higher than the level in the freestream.

This is to be expected since this is a region of uniform flow, having been turned by a straight, oblique shock. The higher fluctuation level is likely due to acoustic radiation from the separated, free shear layer. Further downstream, there is another sharp peak (location 11) behind the rear shock. This location is close to the foot of the rear shock, which has been observed to be highly unsteady.[17,22] The unsteadiness of the rear shock foot is probably caused by its intersection and interaction with the free turbulent shear layer bounding the separation bubble. Aft of location 11, there is another small peak at location 3. This can be explained by the flapping motion of the slip-line which has been observed by Alvi and Settles[17] in their high-speed shadowgrams.

The rms distribution along row E, presented in Fig. 14d, exhibits two peaks with an approximately-constant level between them. The upstream peak (locations 20 and 21) is due to the motion of the separation shock. The peak at location 6 is caused by unsteadiness of the embedded jet shock seen in Fig. 7.

The rms distributions discussed above indicate that the features of the interaction visible in Fig. 7 are all unsteady. In the optical deflectometry measurements this behavior is manifested as increased rms light intensity in the vicinity of these unsteady flow features.

Our measurements also allow us to make some observations about the technique itself. From a comparison of Figs. 6 and 7, it is obvious that the continuous-light shadowgram only shows the large-scale features of the flow; the finer details visible in Fig. 6 are missing. This is due to the fact the continuous-light shadowgram averages or "smooths-out" small-scale fluctuations which have a time scale much smaller than the exposure time (1/30th of a second). The fact that the rms distributions recorded here are fairly constant except in the vicinity of the large-scale features (mainly shock waves) of the mean flowfield indicates that the technique is, for the most part, sensitive only to strong fluctuations which have large density gradients associated with them. A similar technique based on the Schlieren method could be expected to provide greater detail, but that has not been attempted here.

Power Spectra

The rms distributions presented above show that the entire λ-shock structure is unsteady. However, the characteristics of the unsteadiness are different in different parts of the flowfield. Some of these differences can be made apparent by a examination of the power

spectra of fluctuations recorded at various locations in the interaction.

Figs. 15 - 18 present the power spectra along the rows for which the rms distributions were discussed in the previous section. A shadowgram similar to Fig. 7 showing the measurement locations is also included in these figures for convenience.

It can be seen from Fig. 15 that the fluctuations in the freestream flow both upstream and downstream of the "main" shock wave are broadband and are constant over the frequency range measured. The increase in rms levels upstream of the shock (location 9) is mainly in the 0-15 kHz range. We believe this range represents shock oscillation frequencies. At location 6, the entire range of frequencies measured has greater energy but the spectrum is still dominated by "lower" frequencies. The increased energy levels rapidly dissipate downstream of the shock, and the spectrum returns to its original shape.

The freestream spectra along row B (see Fig. 16) are essentially identical to those in row A. The behavior near the triple point, however, is different than in the vicinity of the main shock. The range of frequencies excited extends to approximately 35-40 kHz. The greatest increases in energy are in the 0-10 kHz range, where the spectral level is approximately constant. Also, the decay of the fluctuations aft of the shock wave extends downstream for a considerable distance. This can be seen in the spectrum for location 4, which still has significant energy in the 0-20 kHz range. This may be due to the vicinity of this location to the slip-line, which is known to be unsteady. The intersection of three shock waves and the presence of the slip-line make it difficult to isolate the effects of any particular feature, or to draw more specific conclusions from the data.

Power spectra for locations along row D are shown in Figure 17. It can be seen from the spectra around location 25 that the separation shock excites a broad range of frequencies (up to approximately 35 kHz). Similar increases were observed in the pressure fluctuations measured at the foot of the separation shock as discussed above. The spectra are dominated by extremely large fluctuation levels at very low frequencies. In the "plateau" region between the separation and rear shocks, the spectra are broadband and flat over essentially the entire frequency range (locations 17-20). The rear shock (locations 9-14) causes increases in energy levels over frequencies extending up to 40 kHz. The distribution of energy in the region between the rear shock and the slip-line (locations 4-8) is broadband. The slip-line itself is seen to have greater energy below 6-7 kHz (locations 2-3).

Finally, power spectra for selected locations along row E are presented in Fig. 18. The spectra in the vicinity of the separation shock (locations 19-24) show features that are similar to those of corresponding locations along row D. There is evidence of a peak in the 0-10 kHz range and the spectra are dominated by low frequency fluctuations. Inside the separation bubble (locations 10, 14, 16) the spectra are flat and broadband for the frequencies measured. The imbedded jet shock shows a gradual "roll-off" up to the cutoff frequency, with the lowest frequencies being the most prominent.

The power spectra presented here indicate that the entire shock structure generated by the interaction undergoes relatively low-frequency oscillations. The shock waves excite a broad range of frequencies which quickly dissipate at locations removed from the immediate vicinity of these waves. The separation shock oscillations, in particular, seem to be dominated by very low frequencies.

Impinging Jet Measurements

The rationale for conducting the impinging jet measurements has been discussed above. All the cases measured showed similar features. Therefore, only one representative case will be presented here. This is the case with the jet impinging upon the flat plate at $\alpha = 50^{\circ}$. Figure 19 shows the rms and mean pressure distributions measured for this case. A schematic of the arrangement is also shown in the figure. The "bump" in the distributions between s/D = -1 and s/D = -2 is due to the reflection of the terminating shock wave from the free shear layer which impinges upon the plate surface as an expansion wave. This, in turn, reflects from the plate surface and sets up a series of alternating shock-expansion impingements upon the surface. This is not a present limitation because we are primarily interested in the region near the centerline of the jet close to the stagnation point.

It can be seen that the mean pressure is highest at a location off the centerline of the jet. This is due to the fact that, for a jet impinging upon a flat surface at an angle, the stagnation streamline moves off the jet axis.[23] In all the cases measured, as in the case shown, a peak in the rms distribution is observed slightly displaced from the peak in the mean pressure distribution.

Kuethe *et al*[24] have noted that velocity fluctuations in the vicinity of the stagnation point on blunt bodies in a uniform flow are higher than in the freestream. Their investigation of the flow near the stagnation point indicates that these fluctuations are a result of a random motion of the stagnation point in both subsonic and supersonic flows. We believe the same mechanism is responsible for the observed peak in rms pressure in our case. Conceptually, the movement of the stagnation point may be equated to movement of the mean pressure distribution back-and-forth over a transducer at a fixed location. Since the gradients in mean pressure are high near the stagnation point, such a motion will cause high fluctuating levels to be recorded. Also, since the mean pressure gradient is steeper to the right of the mean pressure peak (see Fig. 19) than to its left, the peak in rms pressure appears to the right of the stagnation point.

We believe this phenomenon is also present in the interactions under study and is responsible for the peak in rms seen slightly upstream of the attachment location in the rms pressure distributions presented in Fig. 9. An examination of the corresponding mean pressure distributions shows that the difference between the mean pressure gradients to either side of the peak is even greater in the interactions than in the impinging jet case. At this point, the proposed connection between the motion of the stagnation point and high rms pressure levels must be considered as an hypothesis. A more detailed examination of the issues involved is necessary before any definite conclusions can be drawn.

CONCLUSIONS

Fluctuating pressure measurements have been made beneath swept SWBLIs generated by sharp fins at angles of attack between 10 and 20 degrees at Mach 3 and 4. The pressure fluctuation levels generated by these interactions had not been extensively studied earlier. Measurements were made across the entire range from front to back of these interactions. Analysis of the data provided distributions of rms pressure fluctuations and their spectral

content. The conclusions reached thus far can be summarized as follows:

1. The class of interactions under study can generate significant aeroacoustic loads on portions of high-speed aircraft. The highest loads are experienced at locations closest to the foot of the fin. These are dominated by low-frequency fluctuations in the range 0-5 kHz, and reach a maximum sound pressure level of 160 dB in the cases studied.
2. The peak rms level in these interactions (when normalized by the freestream static pressure) scales approximately with the Mach number normal to the inviscid shock wave (M_n).
3. The phenomenon of intermittent separation, which has attracted much attention in 2-D interactions, is less significant in swept interactions. Nonetheless, an rms pressure peak associated with motion of the separation shock is observed in the current experiments. The magnitude of this peak scales with the sweep angle of the separation line.
4. High spectral energy levels at low frequencies are observed beneath the "jet impingement" region of these interactions.
5. Distributions of rms pressure levels, when normalized by the local mean pressure, show fluctuation-energy peaks near primary separation and beneath the vortex core.
6. The influence of transducer spatial resolution has been clarified with respect to the detection of intermittent separation in these interactions. Transducers of a size comparable to the incoming boundary layer thickness are unable to detect intermittency, resulting in underestimated rms levels and erroneous probability density functions near separation.
7. The rms distributions and power spectra of surface pressure fluctuations can be related to the observed features of the flowfield off the surface.
8. Caution must be exercised in the choice of coordinate frame for presentation of spectra in order to avoid misconceptions.

In addition to the conclusions reached on the basis of fluctuating pressure measurements in the swept SWBLIs, the supplementary optical deflectometry measurements and the impinging jet experiments have provided us with additional information which is pertinent:

1. The entire lambda-shock structure generated by the interaction undergoes relatively low-frequency oscillations.
2. The separation shock motion displays features distinct from that of the other features of the flow field. Its oscillations are dominated by very low frequencies in the 0-10 kHz range.
3. Fluctuating pressure measurements on a flat surface upon which a supersonic jet is incident at an angle indicate that the phenomenon responsible for high rms pressure levels in the rear portion of swept SWBLIs may be a random motion of the stagnation point corresponding to primary flow attachment.

REFERENCES

1. Lu, F. K., "Fin Generated Shock-Wave Boundary-Layer Interactions," Ph.D. Dissertation, Mechanical Engineering Dept., The Pennsylvania State University, Feb. 1988.
2. Kim, K. S., "Skin Friction Measurements by Laser Interferometry in Supersonic Flows," Ph.D. Dissertation, Mechanical Engineering Dept., The Pennsylvania State University, Dec. 1988.
3. Lee, Y., "Heat Transfer Measurements in Swept Shock Wave/Turbulent Boundary-Layer Interactions," Ph.D. Dissertation, Mechanical Engineering Dept., The Pennsylvania State University, June 1992.
4. Alvi, F. S. and Settles, G. S., "Physical Model of the Swept Shock Wave/Boundary-Layer Interaction Flowfield." *AIAA Journal*, Vol. 30, Sept. 1992, pp. 2252-2258.
5. Settles G. S. and Dolling, D. S., "Swept Shock Wave/Boundary-Layer Interactions," in *AIAA Progress in Astronautics and Aeronautics: Tactical Missile Aerodynamics*, edited by M. Hemsch and J. Nielsen, Vol. 104, AIAA, New York, 1986, pp. 297-379.
6. Settles G. S. and Dolling, D. S., "Swept Shock Wave/Boundary-Layer Interactions - Tutorial and Update," AIAA Paper 90-0375, January 1990.
7. Zheltovodov, A. A., Maksimov, A. I. and Shilein, E. K., "Development of Turbulent Separated Flows in the Vicinity of Swept Shock Waves," *The Interactions of Complex 3-D Flows*, edited by Kharitonov, A. M., Akademia Nauk USSR, Inst. Theor. and Applied Mechanics, Novosibirsk, 1987, pp. 67-91.
8. Dolling, D. S. and Murphy, M. T., "Unsteadiness of the Separation Shock Wave Structure in a Supersonic Compression Ramp Flowfield," *AIAA Journal*, Vol. 21, Dec. 1983, pp. 1628-1634.
9. Dolling, D. S. and Or, C. T., " Unsteadiness of the Shock Wave Structure in Attached and Separated Compression Ramp Flowfields," *Experiments in Fluids*, Vol. 3, 1985, pp. 24-32.
10. Degrez, G., "Exploratory Experimental Investigation of the Unsteady Aspects of Blunt Fin-Induced Shock Wave Turbulent Boundary Layer Interactions," M.S.E. Thesis, Mechanical and Aerospace Engineering Dept., Princeton University, June 1981.
11. Kistler, A. L., "Fluctuating Wall Pressure Under a Separated Supersonic Flow," *Journal of the Acoustical Society of America*, Vol. 36, March 1964, pp. 543-550.
12. Tran, T. T., "An Experimental Investigation of Unsteadiness in Swept Shock Wave/Boundary Layer Interactions." Ph.D. Dissertation, Mechanical and Aerospace Engineering Dept., Princeton University, 1987.
13. Gibson, B. and Dolling, D. S., "Wall Pressure Fluctuations Near Separation in a Mach 5, Sharp Fin-Induced Turbulent Interaction," AIAA Paper 91-0646, Jan. 1991.
14. Schmisseur, J. D. and Dolling, D. S., "Unsteady Separation in Sharp Fin-Induced Shock Wave/Turbulent Boundary Layer Interaction at Mach 5," AIAA Paper 92-0748, Jan. 1992.
15. McIntyre, S. S., Stanewsky, E., and Settles, G. S., " An Optical Deflectometer for Turbulence Measurements," presented at the 14th ICIASF Congress, White Oak, MD, Oct. 27-31, 1991.

16. McIntyre, S. S. and Settles G. S., "Optical Experiments on Compressible Turbulent Mixing Layers," AIAA Paper 91-0623, Jan. 1991.
17. Alvi, F. S. and Settles, G. S., "Structure of Swept Shock Wave Boundary-Layer Interactions Using Conical Shadowgraphy," AIAA Paper 90-1644, June 1990.
18. Laganelli, A. L., Martelluci, A. and Shaw, L. L., "Wall Pressure Fluctuations in Attached Boundary Layer Flow," *AIAA Journal*, Vol. 21, 1983, pp. 495-502.
19. Tan, D. K. M., Tran, T. T. and Bogdonoff, S. M., "Surface Pressure Fluctuations in a Three-Dimensional Shock Wave/Turbulent Boundary Layer Interaction," AIAA Paper 85-0125, Jan. 1985.
20. Erengil, M. E. and Dolling, D. S., "Effects of Sweepback on the Dynamics of Unsteady Separation in Mach 5 Compression Ramp Interactions," AIAA Paper 92-0430, Jan. 1992.
21. Dolling, D. S. and Dussauge, J. P., "Fluctuating Wall Pressure Measurements," Chapter 8, NATO Agardograph No. 315, A Survey of Measurement Techniques in Rapidly Distorted Compressible Boundary Layers, May 1989.
22. Alvi, F. S., "An Experimental Study of Swept Shock Wave/Turbulent Boundary-Layer Interactions," Ph.D. Dissertation, Mechanical Engineering Dept., The Pennsylvania State University, Dec. 1992.
23. Henderson, L. F., "Experiments on the Impingement of a Supersonic Jet on a Flat Plate," *Zeitschrift für angewandte Mathematik und Physik*, Vol. 17, 1966, pp. 553-569.
24. Kuethe, A. M., Willmarth, W. W. and Crocker, G. H., "Stagnation Point Fluctuations on a Body of Revolution," *Physics of Fluids,* Vol. 2, No. 6, pp. 714-716, Nov. - Dec. 1959.

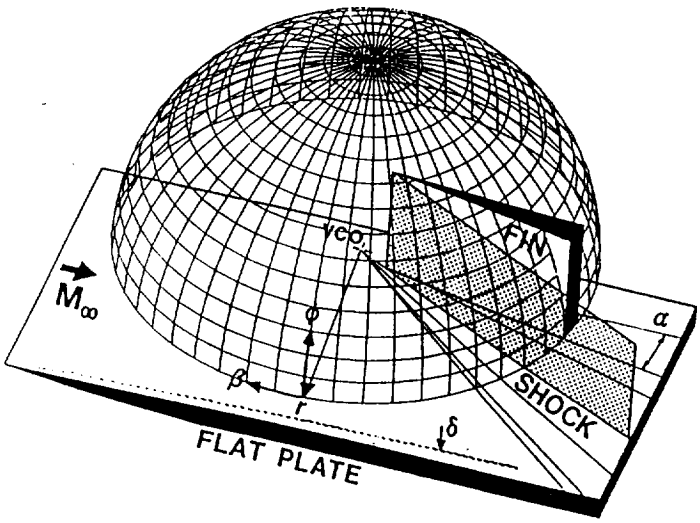

Fig. 1 Spherical polar coordinate frame.

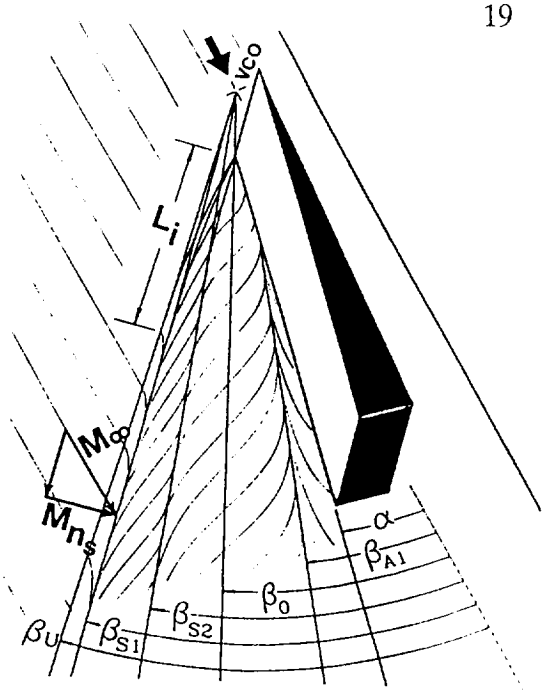

Fig. 2 Sharp fin interaction footprint with nomenclature definitions.

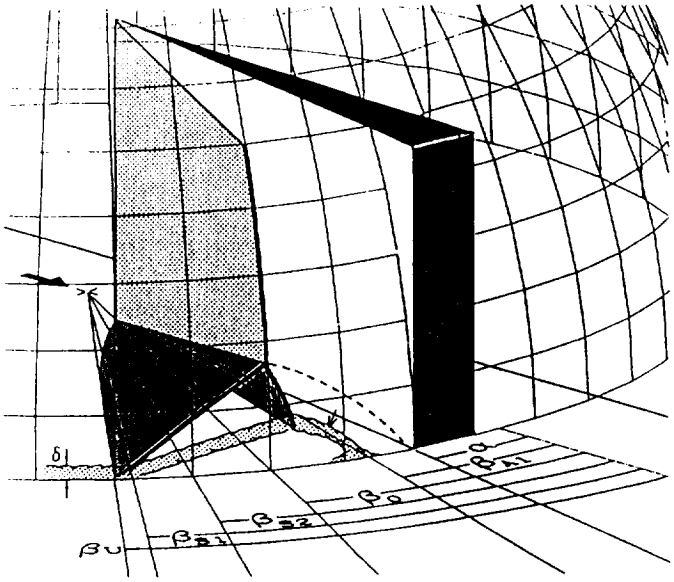

Fig. 3 Projection of quasiconical interaction onto spherical coordinate surface.

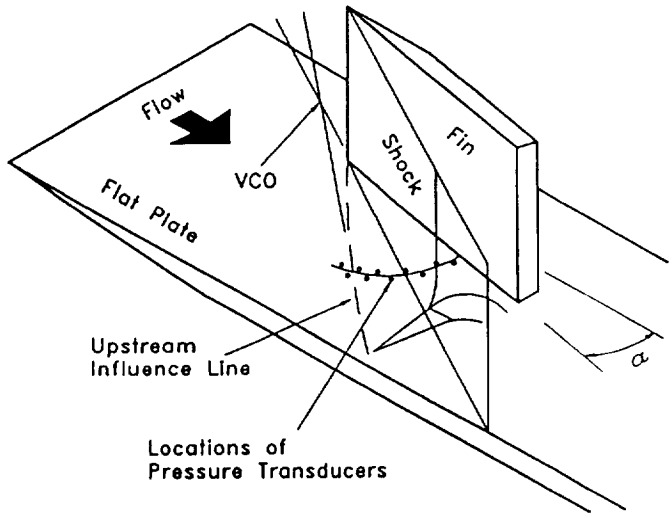

Fig. 4 - Model schematic showing transducer locations

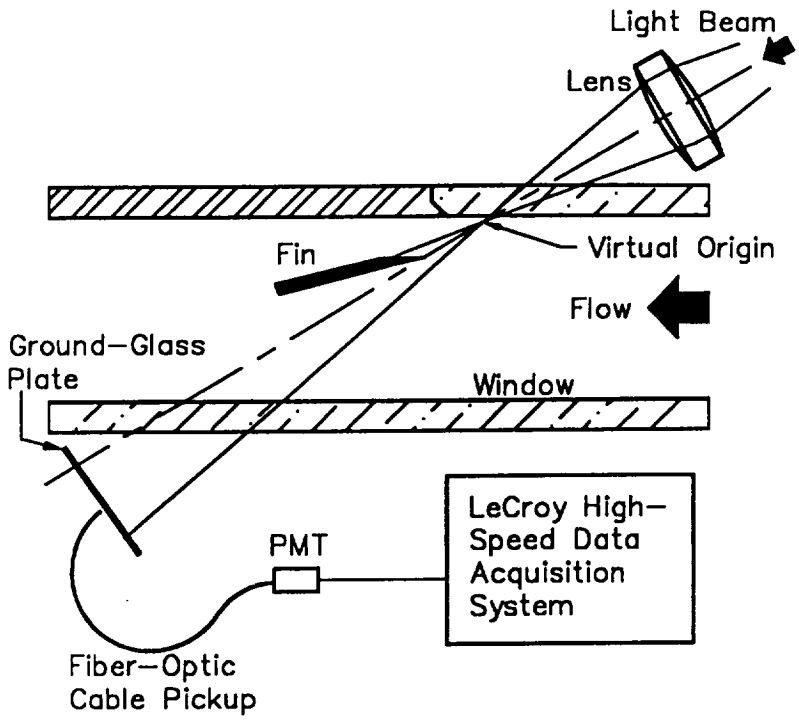

Fig. 5 Conical deflectometry setup

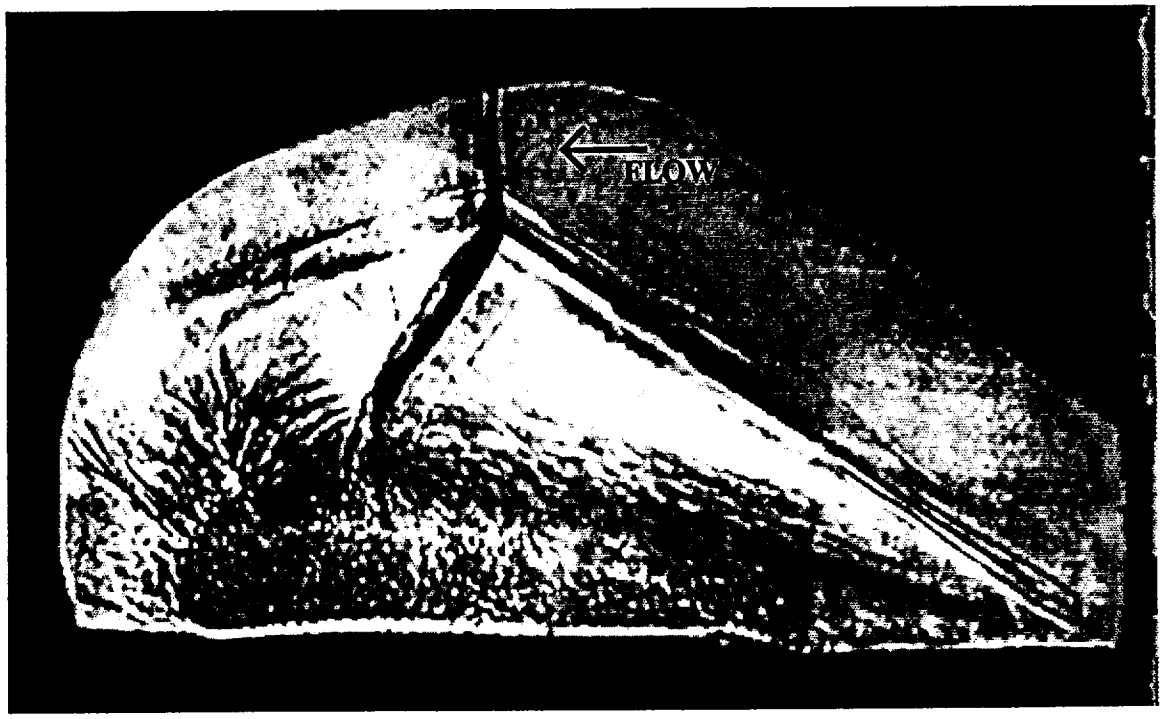

Fig. 6 10 μs-spark conical shadowgram of M = 4, α = 20 deg. interaction. From Ref. 17

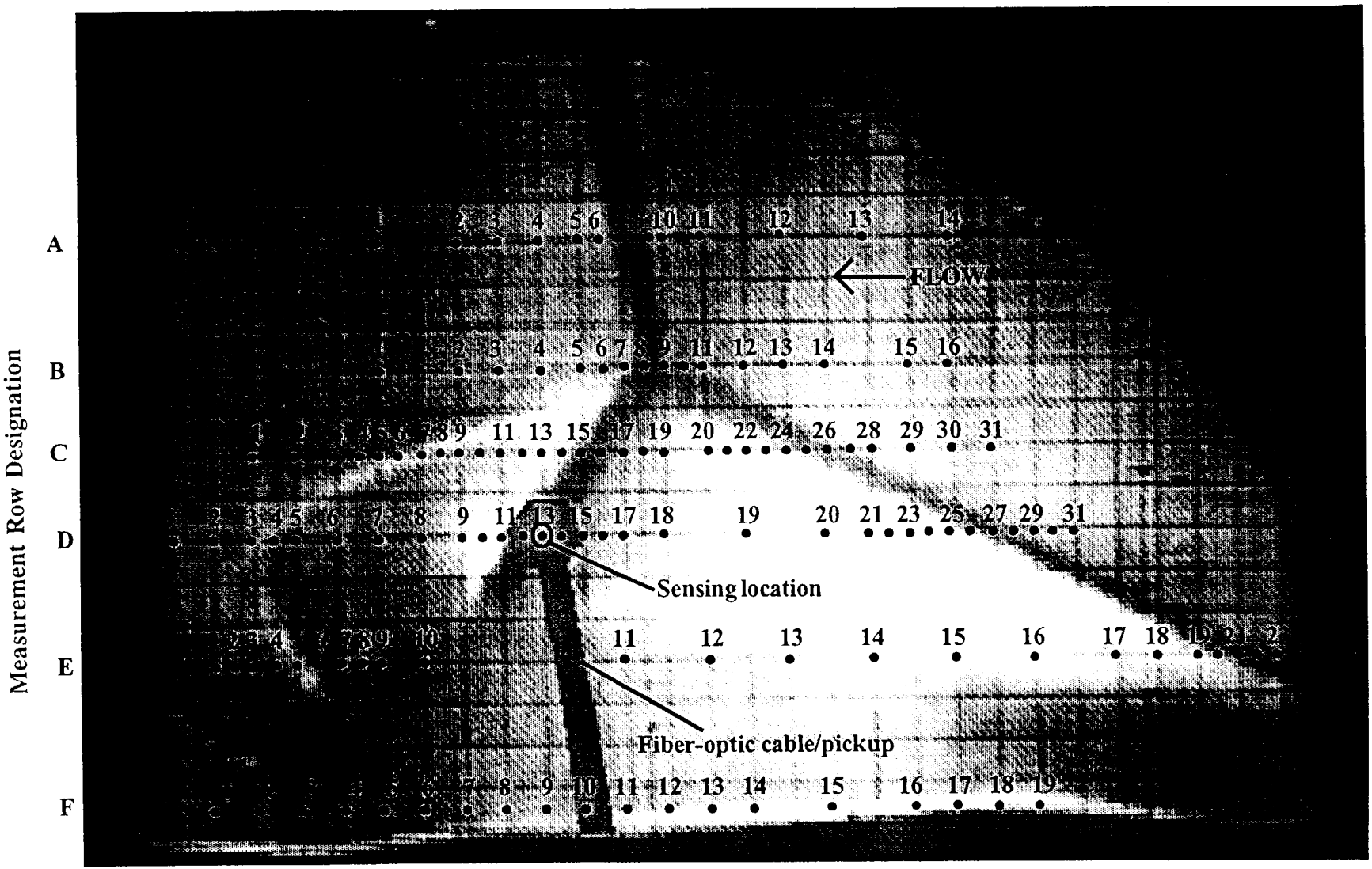

Fig. 7 Continuous-light conical shadowgram of M=4, α = 20 deg. interaction showing Optical Deflectometry measurement locations

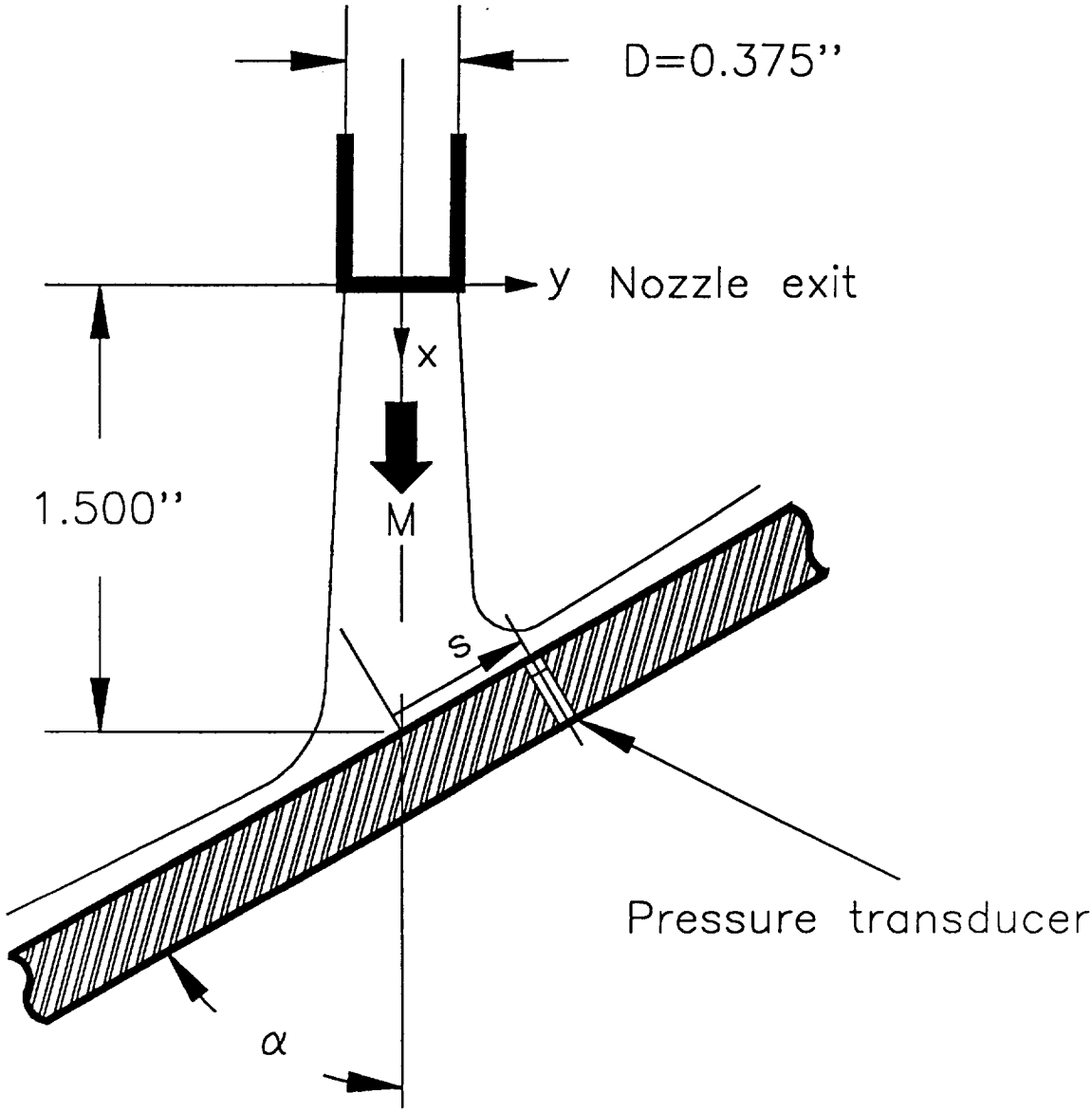

Fig. 8 Setup for impinging jet measurements

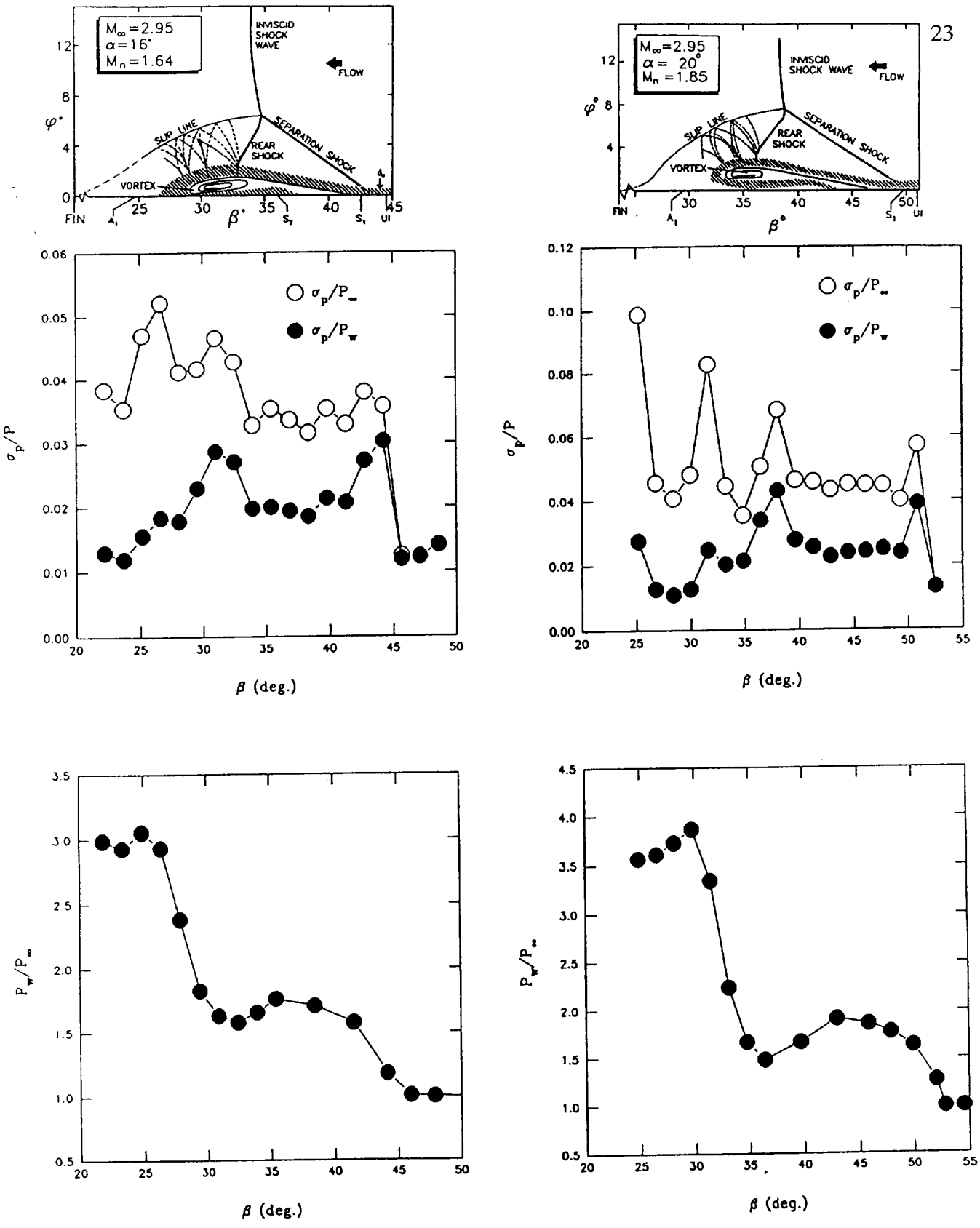

Fig. 9 Flowfield map, rms pressure distributions, and mean pressure distributions (M_∞ = 3 and 4, α = 16 and 20 deg.). Mach number and fin angle indicated on flowfield map.

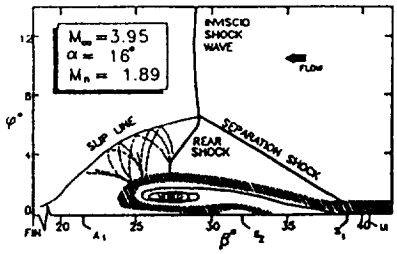

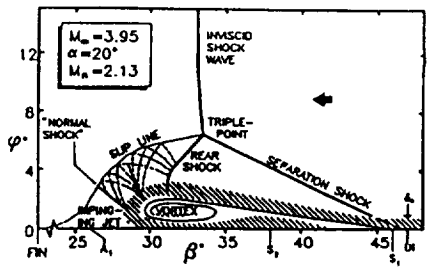

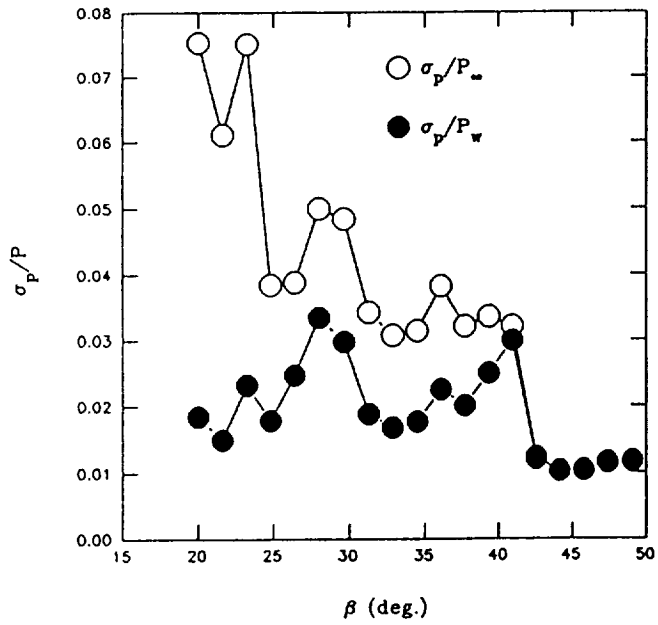

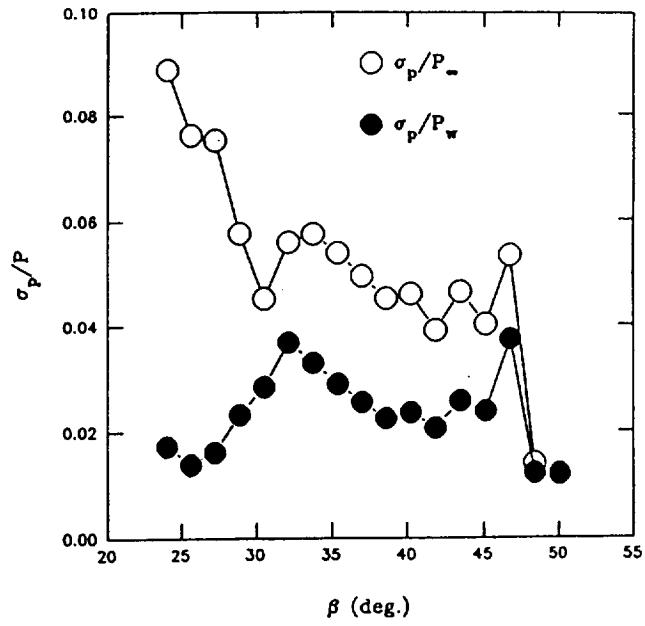

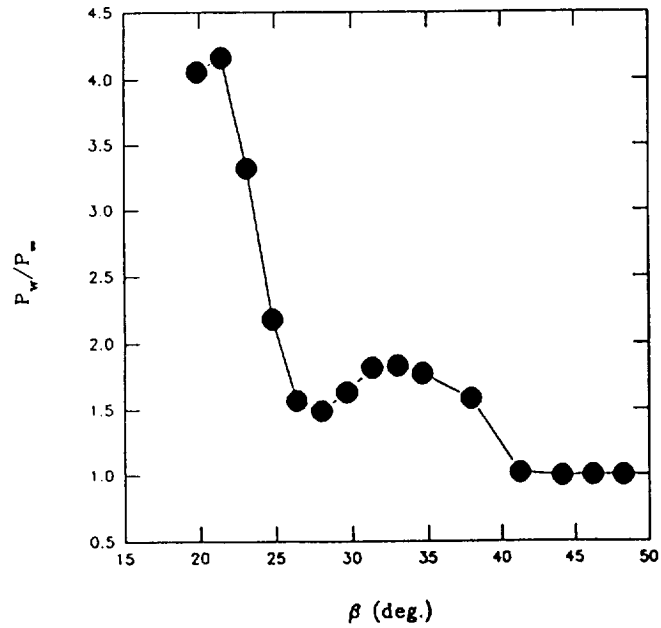

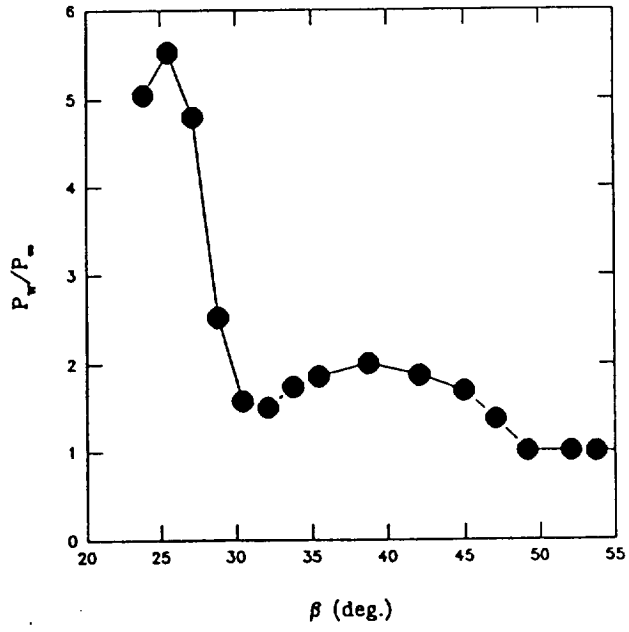

Fig. 9 concluded.

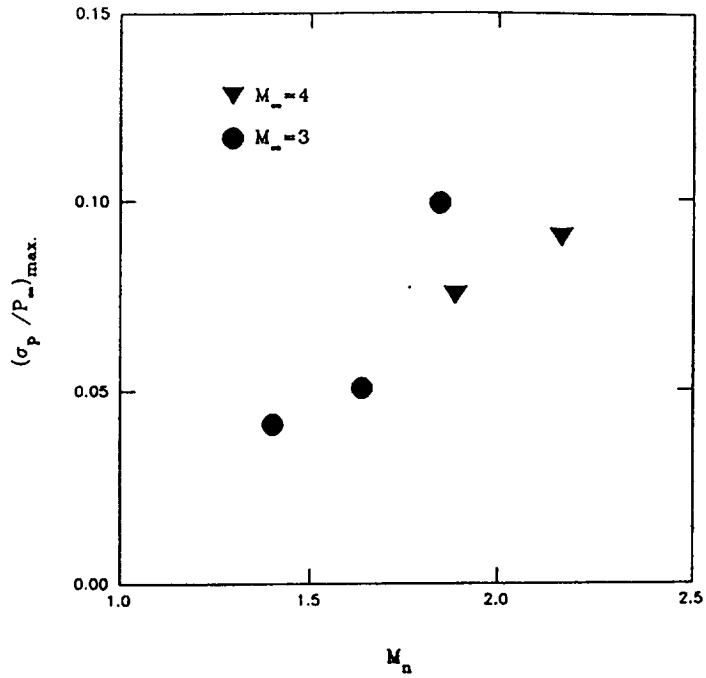

Fig. 10 Maximum rms in interaction as a function of Mach number normal to the shock wave.

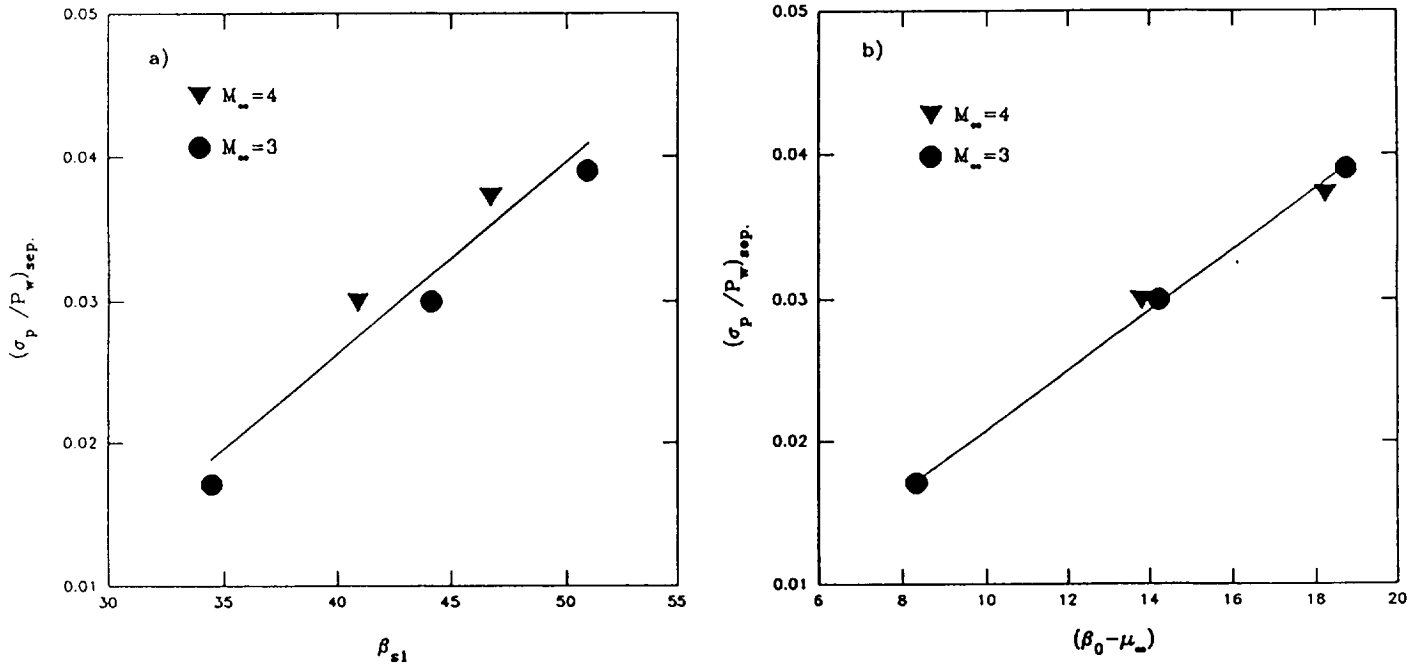

Fig. 11 Maximum rms near primary separation as a function of:
a) Separation line sweep angle, and
b) Shock strength parameter.

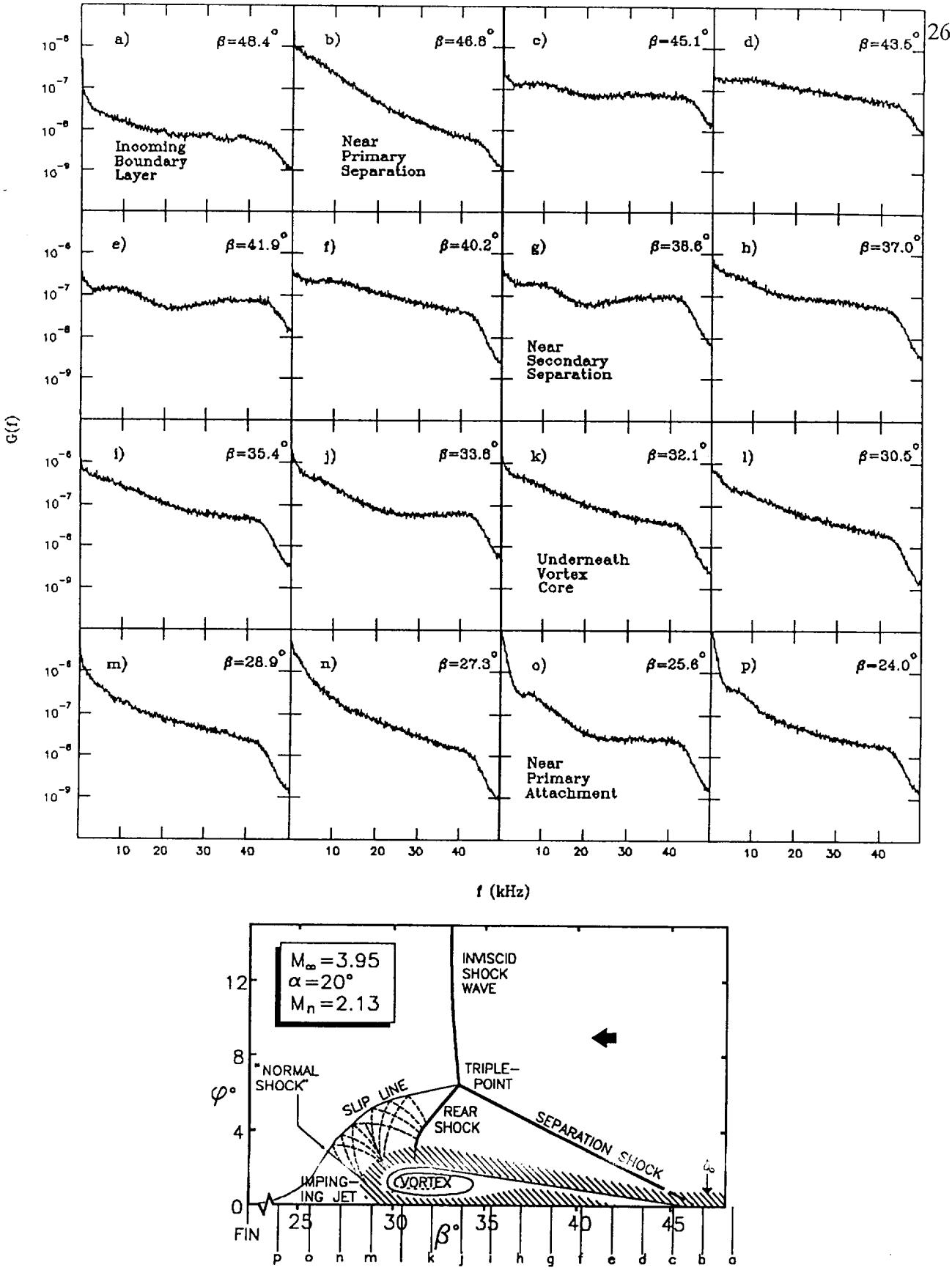

Fig. 12 Power spectra through the interaction for M_∞= 4, α = 20 deg.

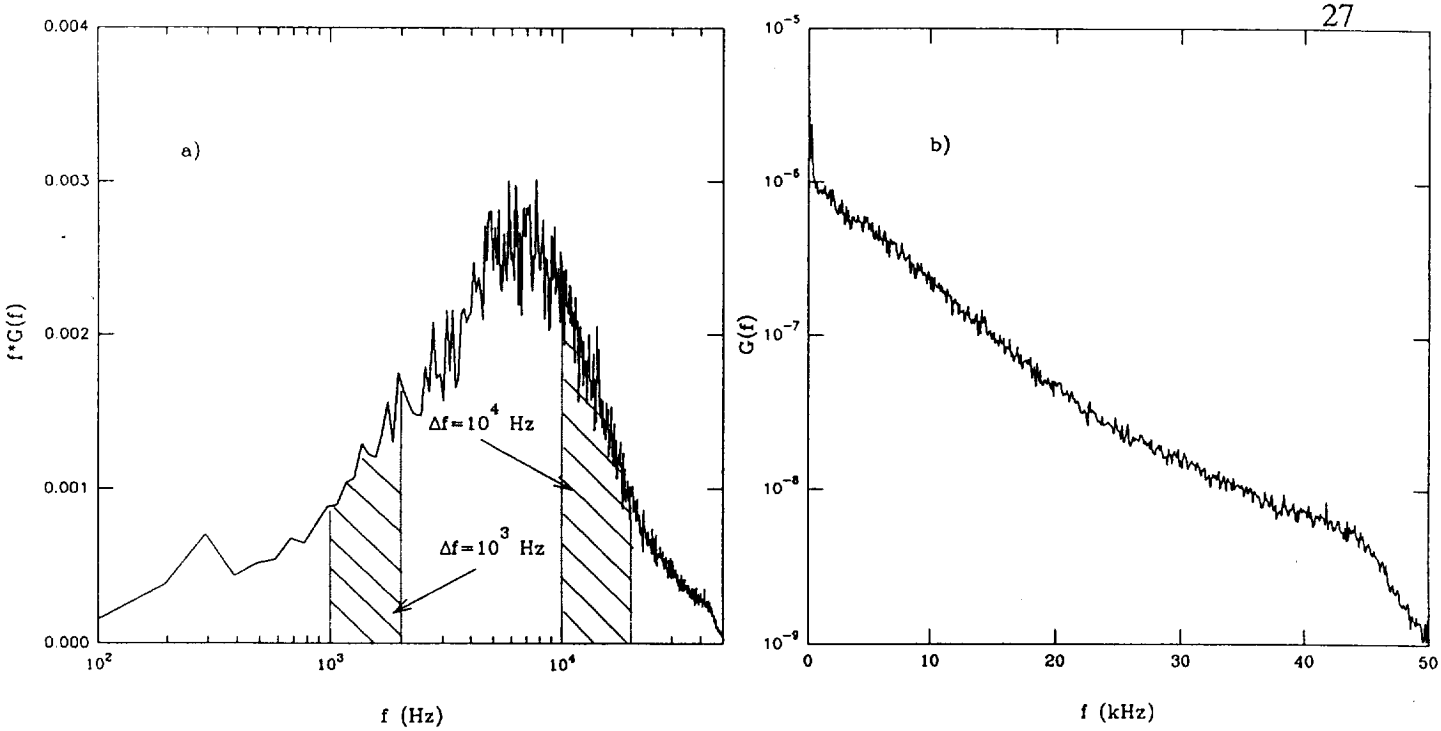

Fig. 13 Comparison of power spectra in different coordinate frames.

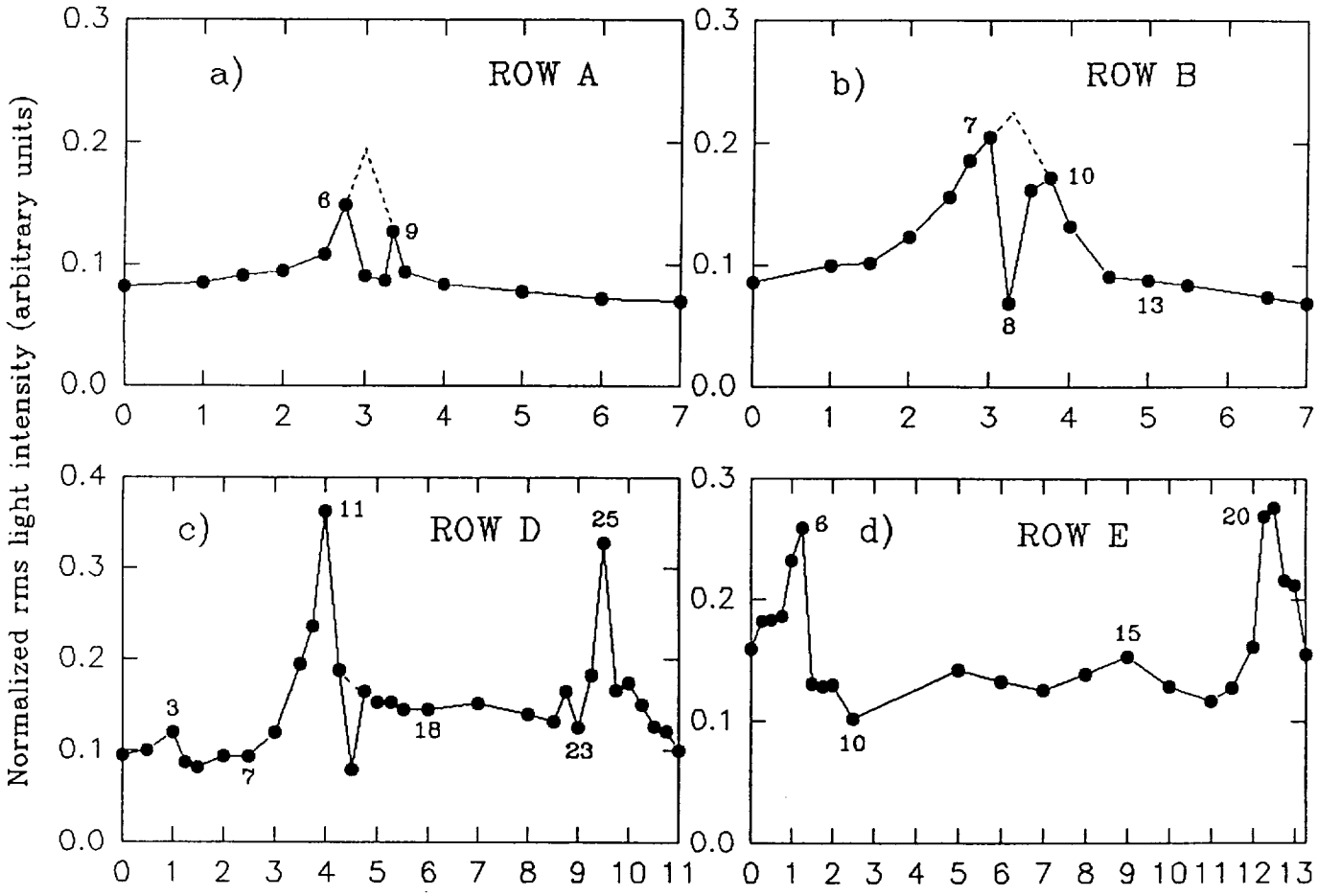

Fig. 14 Distributions of normalized rms light-intensity along various rows. Abscissa is the distance in cm from leftmost location in each row.

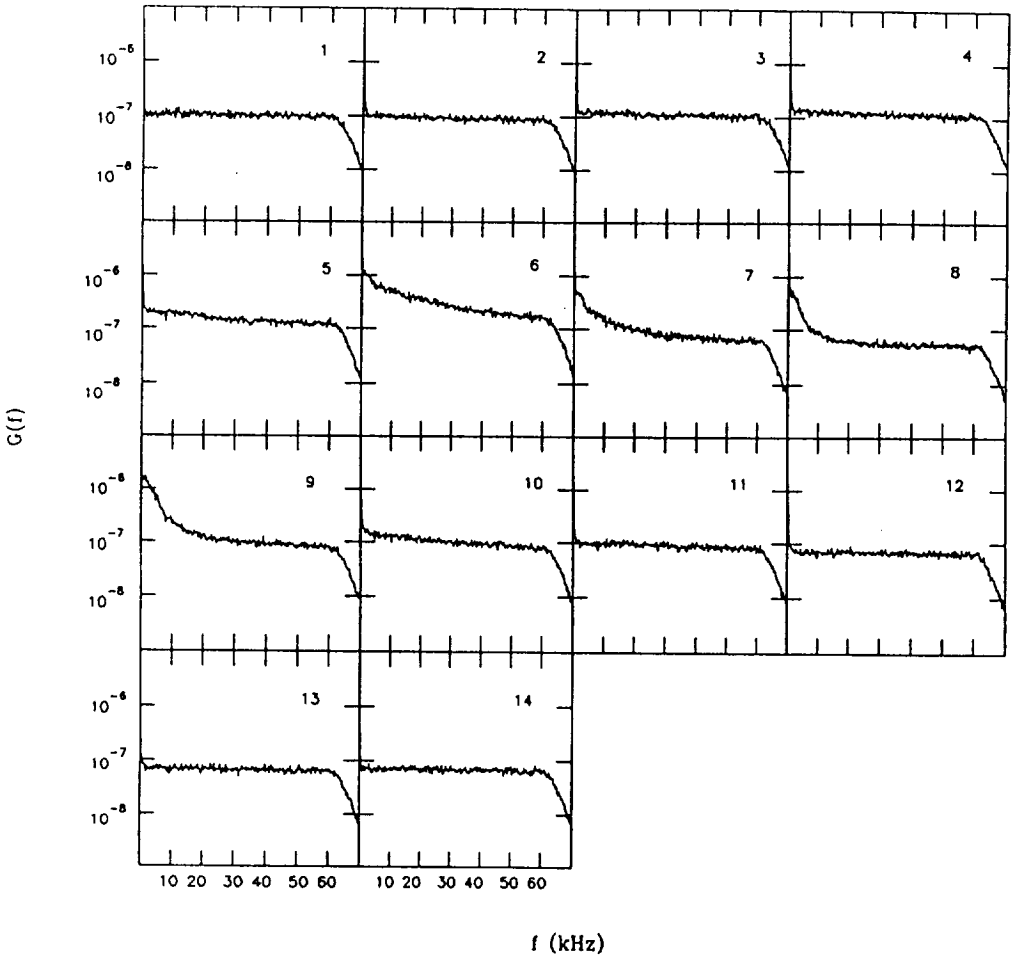

Fig. 15 Power spectra of light-intensity fluctuations along row A.

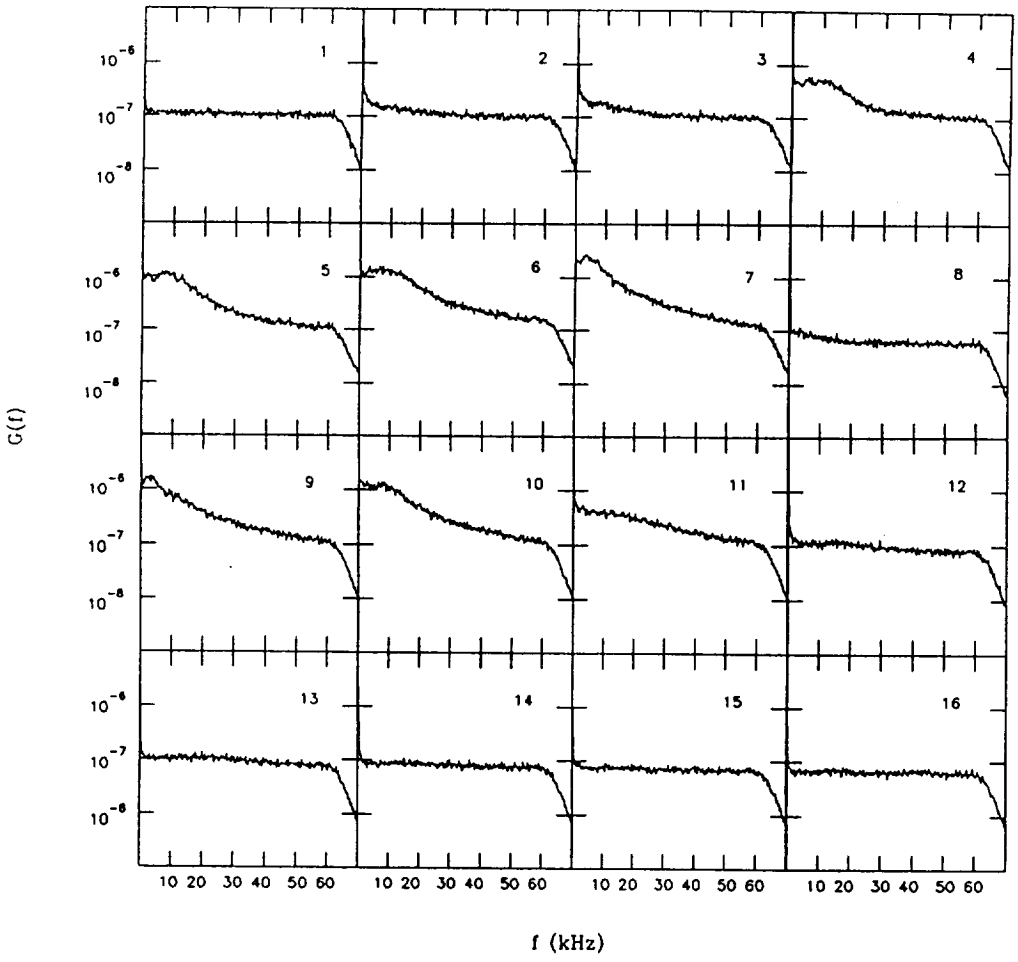

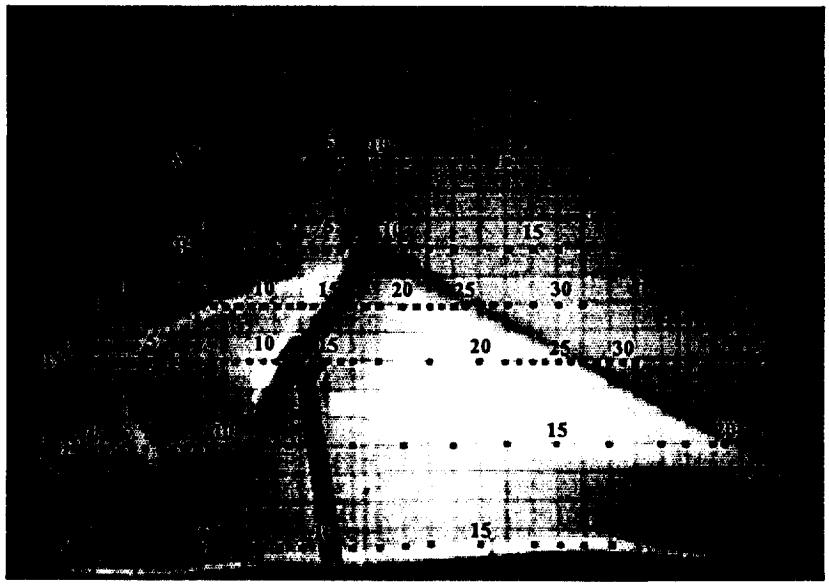

Fig. 16 Power spectra of light-intensity fluctuations along row B.

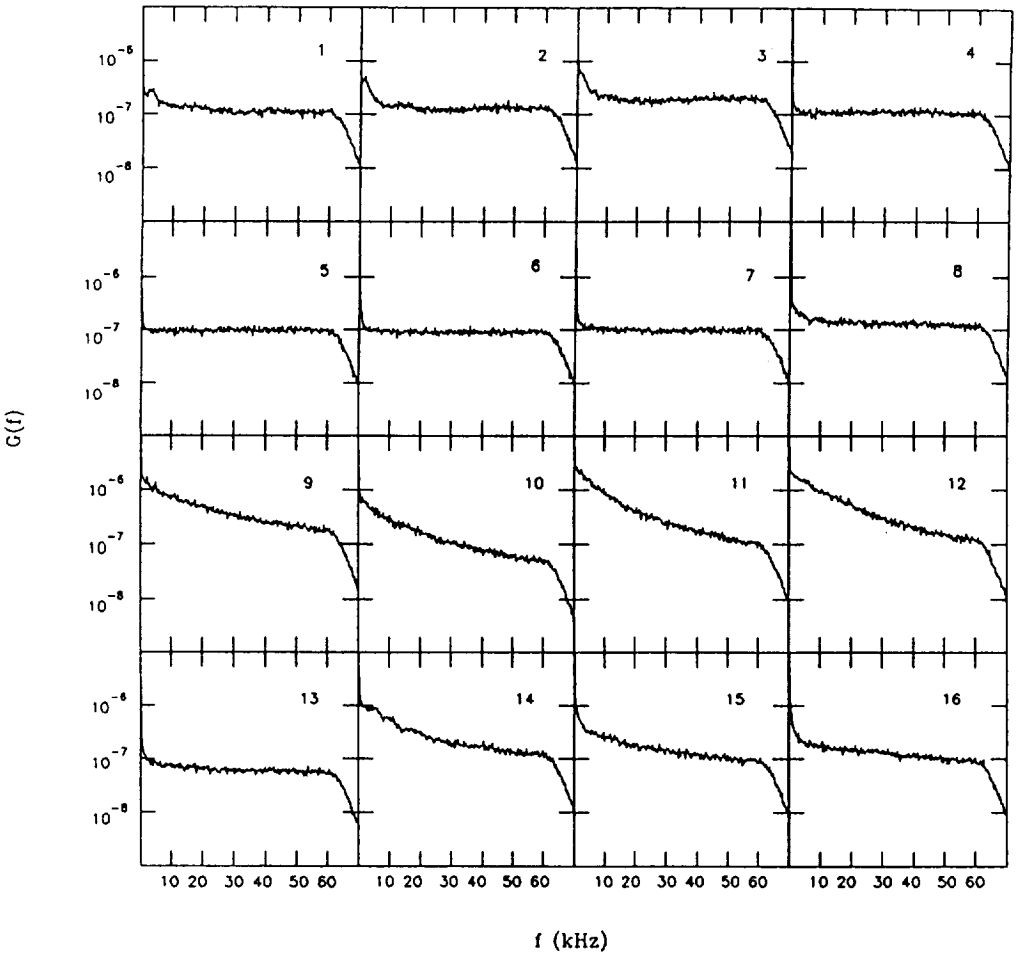

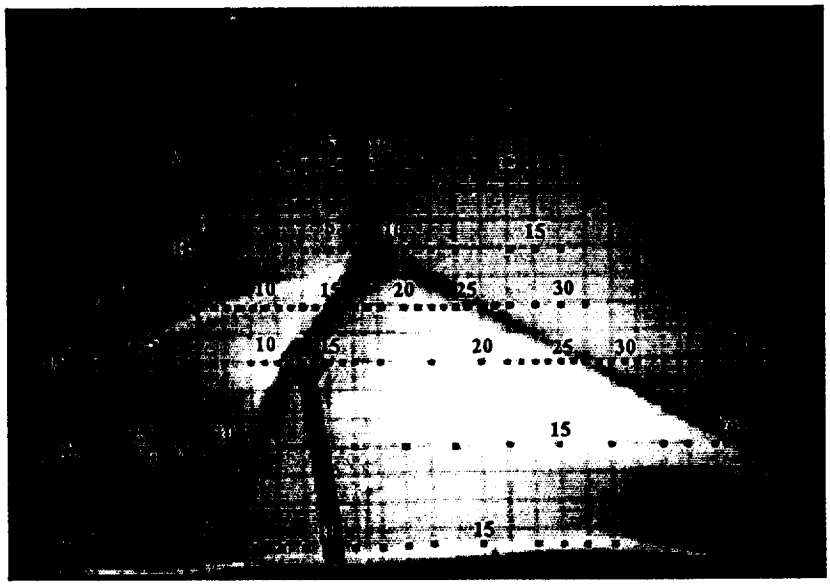

Fig. 17 Power spectra of light-intensity fluctuations along row D.

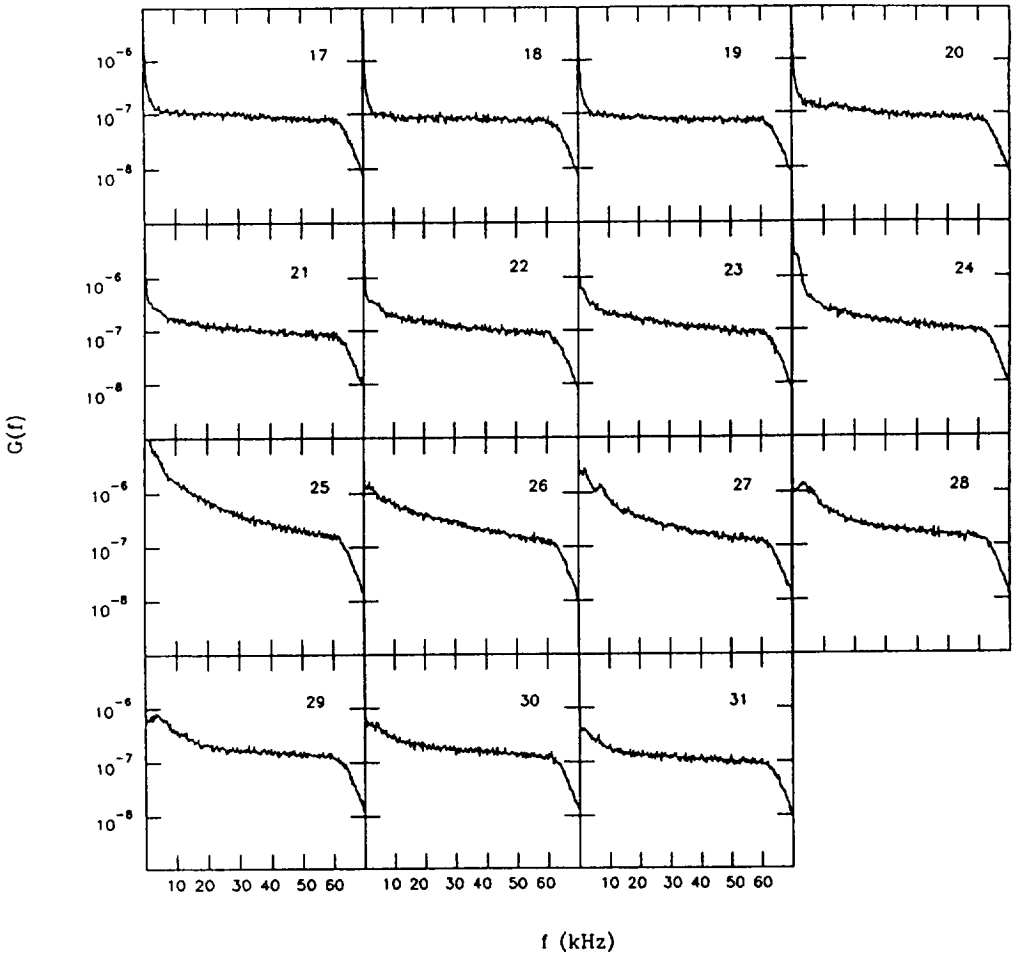

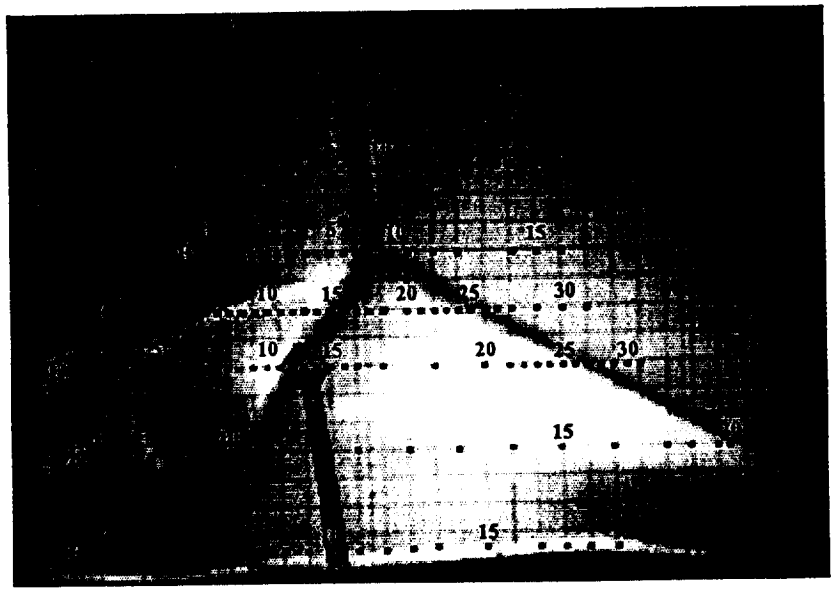

Fig. 17 concluded.

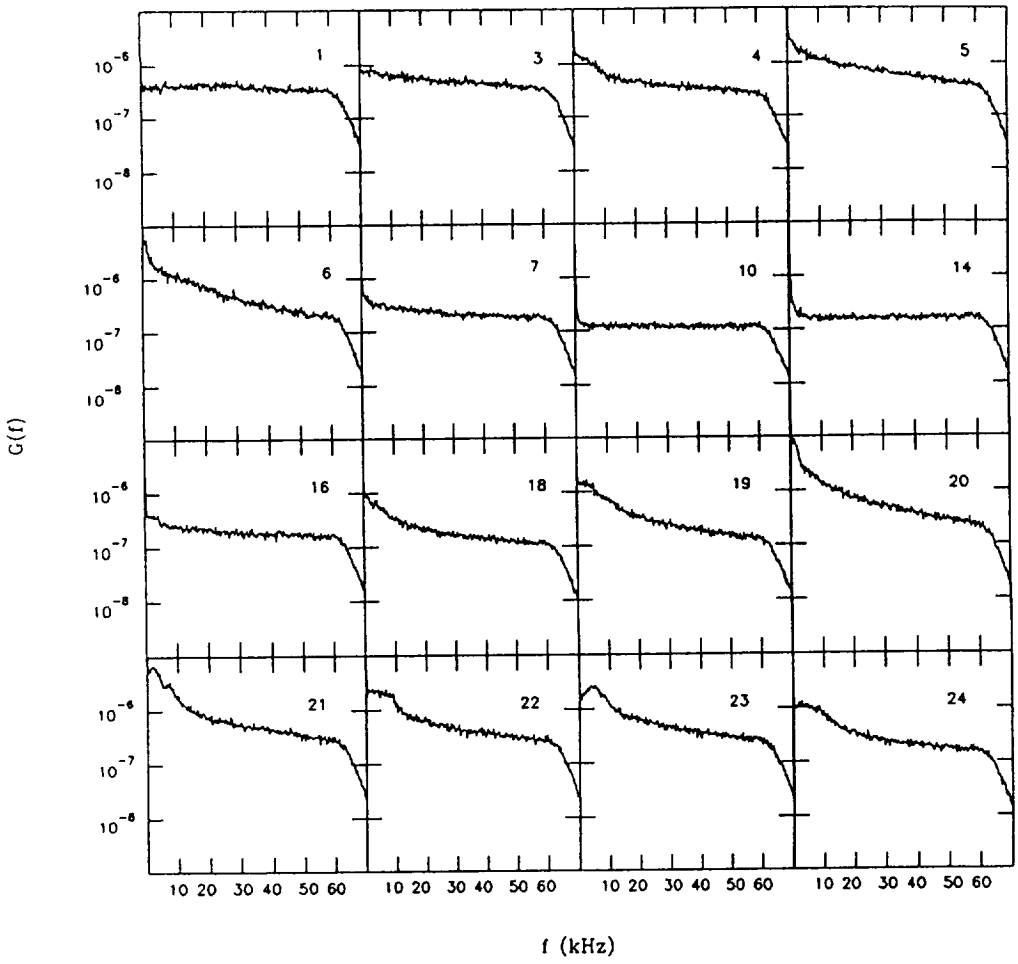

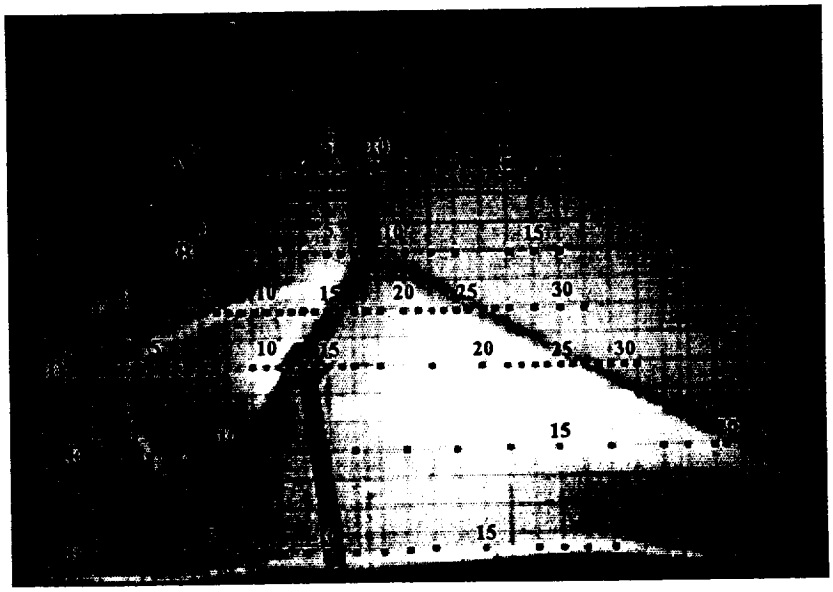

Fig. 18 Power spectra of light-intensity fluctuations along row E.

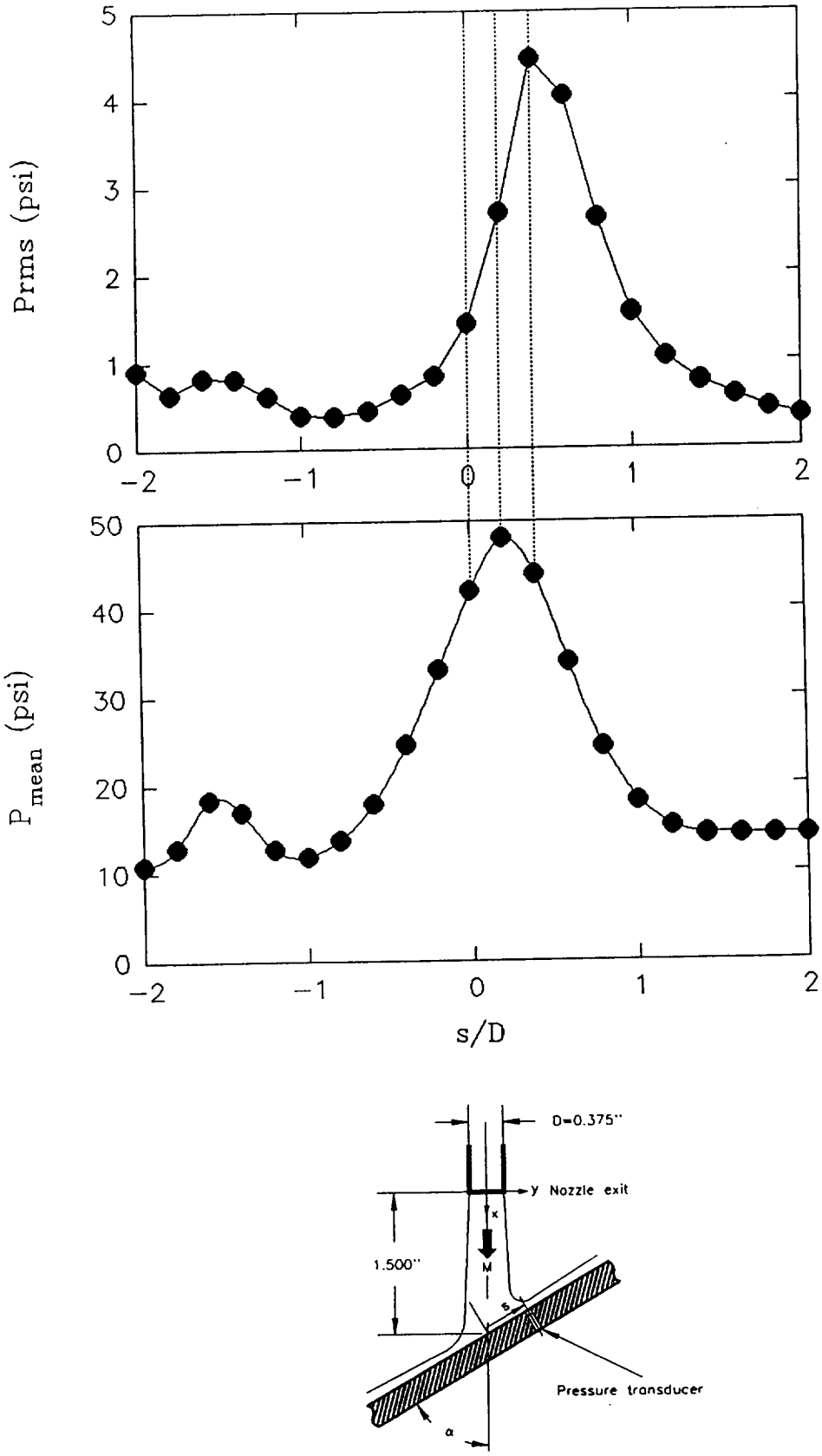

Fig. 19 RMS and mean pressure distributions on the flat plate with a M = 1.65 jet impinging upon it at α = 50 deg.